2022-04-27

Context-Dependent Activation of the A11 in Freely Moving Mice

Thurston, Elizabeth

UNIVERSITY OF CALGARY

Context-Dependent Activation of the A11 in Freely Moving Mice

by

Elizabeth Thurston

A THESIS

SUBMITTED TO THE FACULTY OF GRADUATE STUDIES

IN PARTIAL FULFILMENT OF THE REQUIREMENTS FOR THE

DEGREE OF MASTER OF SCIENCE

GRADUATE PROGRAM IN NEUROSCIENCE

CALGARY, ALBERTA

APRIL, 2022

ABSTRACT

The heterogeneous A11 nucleus is the primary direct source of spinal dopamine in rodents. Previous work has implicated this region in nociception, locomotion, and sociosexual behaviours in various animal models. The A11's activity patterns in freely moving animal models have not been researched. I examined the A11 region's activity through fibre photometry in mice during various behavioural contexts to elucidate this region's roles. I found that the A11 regional activity was most excited by novel stimuli. Goal-directed locomotion was associated with increased A11 activity, while locomotion in the open field was on par with baseline fluorescence levels. During states of lower anxiety in the open arms of the elevated plus maze, I also observed increased A11 activity. The A11's activity was also increased during periods of ultrasonic vocalization. Overall, I suggest that the A11 responds to novelty by promoting goal-directed locomotion and also encodes sociosexual vocalizations. Additionally, I validated an intersectional viral approach to target spinally-projecting A11 cells in a circuit-dependent manner.

Keywords: A11 nucleus, fibre photometry, novelty, locomotion, ultrasonic vocalization

PREFACE

This thesis is original, unpublished, independent work by the author, E. Thurston. A portion of the data in Chapter 1 was reported in abstract form (Thurston et al., 2021).

ACKNOWLEDGMENTS

Firstly, I would like to thank my supervisor, Dr. Patrick Whelan, for his guidance and mentorship. I would also like to thank the funding agencies who have supported me and my work throughout my degree: SCNIP, AGES, Wings for Life, and CIHR. Thirdly, I would like to thank my lab mates and colleagues for the invaluable feedback, support, and listening. I would also like to thank my committee for their guidance. Finally, I would like to thank my support system in Calgary, throughout Ontario, and elsewhere: you have all helped me so much throughout this process, and I am forever grateful.

TABLE OF CONTENTS

LIST OF TABLES

LIST OF ILLUSTRATIONS, FIGURES, AND GRAPHICS

Figures were created with BioRender.com

LIST OF SYMBOLS, ABBREVIATIONS, AND NOMENCLATURE

6-OHDA	6-hydroxydopamine
A11	Aminergic nucleus within the hypothalamus
AADC	Aromatic amino acid decarboxylase
AAV	Adeno-associated virus
AUC	Area under the curve
CGRP	Calcitonin gene-related peptide
ChR2	Channelrhodopsin-2
D_1R	Dopamine receptor D1
D_2R	Dopamine receptor D2
DA	Dopamine
DAT	Dopamine transporter
DREADD	Designer receptors exclusively activated by designer drugs
EPM	Elevated plus maze
GABA	Gamma-aminobutyric acid
GPCR	G-protein coupled receptor
IHC	Immunohistochemistry
IML	Intermediolateral cell column
L-DOPA	l-3,4-dihydroxyphenylalanine
OF	Open field
PBS(T)	Phosphate-buffered saline (with triton)
PFA	Paraformaldehyde
PHA	Posterior hypothalamic area
PT	Posterior tubercular area
RT	Room temperature
TH	Tyrosine hydroxylase
USV	Ultrasonic vocalization
VGLUT2	Vesicular glutamate transporter 2
VMAT2	Vesicular monoamine transporter 2

1. CHAPTER 1: Introduction

1.1. The Goal of this Thesis

Dopamine (DA) serves a variety of roles in the central nervous system, including learning, reward mechanisms, social behaviours, and relevant to this thesis, locomotion (Beninger, 1983; Schultz, 1997; Bharati and Goodson, 2006; Gordon and Whelan, 2006). Dopaminergic systems are primarily localized in the diencephalon and upper mesencephalon (Moore and Bloom, 1978). The canonical view of dopaminergic modulation of locomotion involves indirect pathways; however, the contribution by direct descending hypothalamic dopaminergic neurons to locomotor control is important to investigate. These direct DAergic projections are known to play a role in nociception, with proposed roles in sociosexual or locomotor behaviours. Previous work has implicated many regions within the diencephalon as centres for locomotor control, yet little work has been done to explore the role of the hypothalamic A11 nucleus in locomotor behaviours. The Whelan lab has previously shown that the dopaminergic population of cells within the A11 can produce locomotion (Koblinger et al., 2018). Still, the specific circuit responsible for this behaviour is unknown, which is investigated in this thesis. In addition, the activity profile of the A11 during locomotor and non-locomotor behaviours is of interest. It is explored in this thesis as it may shed light on the A11's biological activity in various contexts.

1.2. The A11 Nucleus

1.2.1. Anatomy and Composition

Within the central nervous system, the aminergic cell groups A1-A12, first described by Dahlström and Fuxe (1964) and subsequently confirmed by Hökfelt et al. (1976), include the A11 nucleus. Later, groups A13-A17 were added (Björklund and Lindvall, 1984; Hökfelt et al., 1984). Aminergic cell groups utilize monoamines such as dopamine, norepinephrine, or serotonin for neurotransmission (Dahlström and Fuxe, 1964).

The dopaminergic A11 cell group has been identified in a wide variety of species: human, non-human primate, mouse, rat, guinea pig, zebra finch, quail, dog, cat, sheep, crocodile, and a more basal A11 equivalent has been identified in the zebrafish (Hökfelt et al., 1976; Skagerberg and Lindvall, 1985; Tillet, 1994; Holstege et al., 2003; Okura et al., 2004; Charlier et al., 2005; Bharati and Goodson, 2006; Qu et al., 2006; Barraud et al., 2010; Lambert et al., 2012;

Billings et al., 2020). This nucleus is found in the rostral posterior hypothalamus and in mice, this small cell group is composed of cells approximately 20 μm in diameter which are multipolar or triangular in shape (Qu et al., 2006). Previous studies have counted approximately 450 tyrosine hydroxylase (TH)-positive DAergic cells in the rat and approximately 130 TH-positive DAergic cells in mice with 40 to 60% of cells projecting to the thoracolumbar spinal cord (Ondo et al., 2000; Qu et al., 2006; Pappas et al., 2010). The descending A11 cells project to all spinal cord segments but the number of cells increases while progressing caudally through the rostrocaudal extent of the nucleus (Qu et al., 2006).

Previous work by the Whelan lab has demonstrated that the A11 DAergic cells in mice are not canonical. While they express TH, AADC, and VMAT2, they do not express DAT (see section 1.3.1 for details about DA synthesis) (Koblinger et al., 2014). Additional work in mice also demonstrated that spinally-projecting A11 cells do not contain D_2 autoreceptors (Pappas et al., 2008). The lack of DAT and D_2 autoreceptors in mice suggests that the A11 cannot limit DAergic activity through canonical autoregulation mechanisms (Pappas et al., 2008; Koblinger et al., 2014). As a result, DA released in the spinal cord may modulate spinal neurons for longer periods (Koblinger et al., 2014). In non-human primates, the A11 cells are monoenzymatic for TH, as they are both AADC- and DAT-negative (Barraud et al., 2010). The enzymatic capabilities of this cell group suggest that the A11 cells are the primary source of spinal L-DOPA in non-human primates (Barraud et al., 2010).

In rodents, research has shown that the A11 is composed of dopaminergic, glutamatergic, and GABAergic cells (Kawano et al., 2006; Abdallah et al., 2015; Fougère et al., 2021; Yamaguchi et al., 2021). A subpopulation of A11 TH-positive cells is also positive for vesicular glutamate transporter 2 (VGLUT2) throughout the nucleus. However, there are more double-immunopositive cells in the rostral extent of the nucleus (Kawano et al., 2006). In rats, 38% of TH-positive cells are positive for VGLUT2, demonstrating that the A11 DAergic cells also maintain the ability to package glutamate into vesicles (Kawano et al., 2006). In mice, 90% of TH-positive cells were VGLUT2-positive, though this method was only able to determine the lifetime presence of VGLUT2, rather than current protein or mRNA presence (Fougère et al., 2021). In rats, GABAergic cells are more numerous in the rostral to middle portion of the A11 (Yamaguchi et al., 2021). Additionally, the caudal aspect of the rat A11 expresses $GABA_B$ receptors in a small number of cells (Wirtshafter and Sheppard, 2001). Further work in rats

demonstrated the A11 labels positively with calretinin (a calcium binding protein) and calcitonin gene-related peptide (CGRP; a neuropeptide and vasodilator) markers (Rogers, 1992; Orazzo et al., 1993; Charbit et al., 2009; Russell et al., 2014).

The Subparafascicular Nucleus

In rats, the subparafascicular nucleus is considered a part of the A11 region; however, there are differences between subparafascicular nucleus and A11 cell types in mice arguing against this claim, or suggestive of species-specific anatomical differences (Takada et al., 1988; Nevue et al., 2016). Work by Charbit et al. (2009) in rats shows that the A11 is both CGRP- and TH-positive, while subparafascicular nucleus cells are only CGRP-positive, though more recent work disproves this discrepancy (Abdallah et al., 2015; Yamaguchi et al., 2021). The unique morphology of A11 cells suggests that the A11 and subparafascicular nucleus cells can be differentiated based on morphology and immunohistochemical methods (Sharma et al., 2018).

Due to the lack of clarity in subparafascicular nucleus /A11 distinction in the literature, I will consider all TH-positive, large, multipolar cells within the A11 as being the defining borders of this region (approximately between bregma -2.06 mm to -2.56 mm within the Allen Brain Atlas) (Franklin and Paxinos, 2008). Specifically, between the caudal border of the A13 where cells are smaller and more compact, and the rostral periaqueductal gray where the posterior commissure above the periaqueductal gray is present at bregma -2.70 mm and serves as a definitive landmark of the periaqueductal gray. This is a more conservative regional differentiation between caudal A11 and the rostral periaqueductal gray than the limits set forth by Pappas et al. (2010), suggesting the A11 occupies the space between bregma -1.90 and -3.0mm, and in line with previous work published by the Whelan lab (Koblinger et al., 2014; Sharma et al., 2018). This definition will encompass any glutamatergic and GABAergic neurons within the confines of the A11.

1.2.2. The A11's Connectome

The A11 nucleus, found in the rostral posterior hypothalamus, was first identified in 1964 but its connectome is still not fully defined. A few connections are well known: the A11 has direct efferents to the prefrontal cortex, the locus coeruleus, and the amygdala (Takada et al., 1988; Takada, 1990; Koblinger, 2017). The A11 also innervates the dorsolateral periaqueductal gray, and in rats, projects to the locus coeruleus, the bed nucleus of the stria terminalis, the

central amygdaloid nucleus, the dorsal raphe nucleus, and the thalamus (Maeda et al., 1991; Peyron et al., 1995; Hasue and Shammah-Lagnado, 2002; Kagan et al., 2013; Messanvi et al., 2013). Recent work suggests that the A11 is the primary dopaminergic input to the medullary reticular formation (Grams et al., 2021).

The only research that defined rat A11 afferents, by Beckford (2008), found that the cingulate, infralimbic, and perirhinal cortical areas (the infralimbic cortex), as well as the subiculum of the hippocampus, the amygdala, lateral septum, bed nucleus of the stria terminalis, parabrachial nucleus, in addition to several thalamic nuclei and hypothalamic areas, project to the A11. A dense projection onto the A11 from the nucleus tractus solitarius was found, where close to 50% of A11 cells were labelled (Beckford, 2008). The rostral A11 is highly innervated by the lateral septum, while the caudal A11 appears to be more significantly innervated by the parabrachial nucleus. Van den Pol (1986) demonstrated that there are likely GABAergic projections onto the A11 region.

Other work reported that the posterior hypothalamic area (encompassing the A11) receives inputs from the subthalamus, brainstem, limbic forebrain, subcortical visual regions, and hypothalamus (Abrahamson and Moore, 2001). A caveat to this work is that only the rostral A11, at most, was included based on bregma points chosen. In addition, the rat subparafascicular region [a subregion of the A11 (see section 1.2.1)] projects to the brainstem, specifically to the periaqueductal gray, reticular formation, superior colliculus, intercollicular region, peripheral shell region of the inferior colliculus, cochlear nuclei, superior paraolivary nucleus, cuneiform nucleus, and inferior olive (Yasui et al., 1992). An interesting possibility is that the subparafascicular mediates acoustic and somatosensory signals based on its afferent connections (Yasui et al., 1992).

There is broad consensus on the A11's direct projections to the spinal cord in many species, including zebrafish, rats, mice, and non-human primates (Skagerberg et al., 1982; Takada et al., 1988; Takada, 1993; Qu et al., 2006; Lambert et al., 2012; Koblinger et al., 2014; Sharma et al., 2018). Research has shown that this nucleus innervates the spinal cord at all levels in the dorsal gray matter and intermediolateral cell column, with fibres also projecting to the ventral horn, and that a cell can project to both the spinal cord and the neocortex (Lindvall et al., 1983; Cechetto and Saper, 1988; Takada et al., 1988). A non-specific lesion of the midbrain (containing the A11) led to a decrease in spinal DA concentrations in rats (Mouchet et al., 1982).

Of the A11 descending projections in the rat, the majority (> 90%) extend ipsilaterally, while up to 10% project contralaterally (Skagerberg and Lindvall, 1985). Specifically examining the non-DAergic cells within the A11, there is the crossing of these projections approximately half of the time (Skagerberg and Lindvall, 1985). In non-human primates, the A11's projections to the spinal cord also appear to be mostly ipsilateral (Barraud et al., 2010). These spinally-projecting A11 cells were shown to have long branching processes which extend into multiple spinal segments, demonstrating that the DA released by the A11 can act across various levels of the spinal cord (Skagerberg and Lindvall, 1985). Though work by Qu et al. (2006) found that 5-10% of A10 cells have spinal DAergic projections in the mouse, and despite work in the rabbit showing that both the aminergic A11 and A13 nuclei have projections down to the spinal cord, A11 DAergic cells form the majority of spinally projecting neurons and *the A11 region provides the primary direct source of DA to the spinal cord in rodents and non-human primates* (Dahlström and Fuxe, 1964; Blessing and Chalmers, 1979; Qu et al., 2006; Barraud et al., 2010; Koblinger et al., 2018; Sharma et al., 2018).

1.2.3. The Sexual Dimorphism of the A11 Nucleus

There are clear sex differences concerning the A11, where male C57BL/6 mice have increased lumbar DA concentrations and have more TH-positive cells (Pappas et al., 2010). TH-positive cells were greater in the caudal, but not rostral, A11 in the male mouse (Pappas et al., 2010). Sex-related differences in mouse A11 function are probable but have not been investigated. Work examining the A11 in birds and proposing its involvement in sociosexual behaviours is highlighted in section 1.2.4.4.

1.2.4. Diverse Roles of the A11

1.2.4.1. Locomotion

Using a TH-Cre mouse model, photostimulation of DAergic cells within the A11 evokes locomotor behaviours, albeit with a delay (Koblinger et al., 2018). This is contrary to results found following the optogenetic or chemogenetic activation of A11 cells in a DAT-Cre mouse line, where locomotor behaviours were not significantly altered; however, this method inappropriately targets A11 DAergic cells as they are DAT-negative (Koblinger et al., 2014; Liu et al., 2019). When exposed to novel environments, highly active rats had higher numbers of

TH-positive cells in the A11 to A15 cell groups compared to less active rats (Jerzemowska et al., 2014). These findings propose the A11 as an effector of locomotion.

As a result of the direct connection between the A11 and the spinal cord, neuromodulators or neurotransmitters can act directly on locomotor central pattern generators (neurons within the central nervous system responsible for patterned behaviours such as walking) found in the ventral spinal cord (Duysens and Van de Crommert, 1998; Madriaga et al., 2004; Han et al., 2007; Goulding, 2009; Sharples et al., 2014). Spinal dopamine is known to modulate motor networks within the cord through studies performed on many model organisms, including the leech, lamprey, tadpole, zebrafish, and mouse (Harris-Warrick and Cohen, 1985; Whelan et al., 2000; Madriaga et al., 2004; Christie and Whelan, 2005; Puhl and Mesce, 2008; Thirumalai and Cline, 2008; Sharples et al., 2014; Picton and Sillar, 2016). Both D_1-like and D_2-like DA receptors are present throughout the spinal cord and work has shown that exercise in rats is linked to an increase in DA concentration in the ventral horn of the cord (Gerin and Privat, 1998; Sharples et al., 2014). Studies performed on isolated mouse spinal cord preparations have shown that when monoamines such as DA are bath-applied onto the cord, the thoracolumbar cord is the main region for locomotor rhythmogenesis (Christie and Whelan, 2005).

This direct DAergic circuit from the A11 to the spinal cord is the proposed mechanism underlying increased locomotion following photostimulation of A11 cells (Koblinger et al., 2018). It is important to note that the A11 does send direct DAergic projections to other locomotor regions, specifically the medullary reticular formation, which contains projections to the cervical and lumbar spinal cord (Kim et al., 2017; Grams et al., 2021). The medullary reticular formation has been established as a region capable of producing locomotion during electrical stimulation, and more recent work showed that spinally-projecting medullary reticular formation cells are involved in stopping or turning behaviours (Noga et al., 1988; Whelan, 1996; Kiehn and Dougherty, 2013; Bouvier et al., 2015; Cregg et al., 2020). Therefore, it is not known whether the A11's direct spinal cord projections are responsible for the increase in locomotor activity observed during previous photostimulation experiments, or if this behaviour is due to its supraspinal connections to other locomotor regions (Koblinger et al., 2018). One of the two aims of this thesis is to determine whether the A11-spinal cord connection can elicit locomotor behaviours.

1.2.4.2. Restless Leg Syndrome

Restless leg syndrome, also known as Ekbom Syndrome, is characterized by a need to move the limbs to diminish unpleasant limb sensations at rest, especially in the nighttime (Clemens et al., 2006). Standard treatments for restless leg syndrome utilize dopamine agonists such as ropinirole, pramipexole, and rotigotine (Gossard et al., 2021). Dysfunction of the A11 cell group could contribute to restless leg syndrome; lesioning of the A11 via 6-hydroxydopamine (6-OHDA) found that mice show increased wakefulness, increased locomotion, less time spent sleeping, more episodes of upright standing, and increased limb movements (Ondo et al., 2000; Clemens et al., 2006; Qu et al., 2007; Zhao et al., 2007; Esteves et al., 2016). Conflicting work in human autopsies of restless leg syndrome-afflicted patients shows no difference in A11 volume compared to controls, suggesting potential species differences in the A11's contribution to restless leg syndrome symptoms (Earley et al., 2009).

1.2.4.3. Nociception and Sensory Stimuli

Several lines of evidence illustrate the A11's role in nociception. Early work in rats and cats focused on the A9 and A11 groups and their DAergic inputs onto the dorsal horn of the spinal cord (Fleetwood-Walker et al., 1988). They demonstrated that the electrical stimulation of the A11, but not A9, has antinociceptive effects on the dorsal spinal cord (Fleetwood-Walker et al., 1988). Following 6-OHDA ablation of the A11, the sensory threshold (both thermal and mechanical) is reduced (Wang et al., 2005). In addition, lesioning the A11 increases sensitivity to both noxious and innocuous stimuli (Charbit et al., 2011). The authors suggest that the A11 descending DAergic projections modulate the trigeminocervical complex, and therefore hypothesized that the A11 is involved in migraine (Charbit et al., 2011). When the A11 is inactivated or partially lesioned, pain responses to facial formalin injections are inhibited (Abdallah et al., 2015). In other work, the ablation of the A11 increases trigeminal pain suggesting that the A11's role in nociception is still not clear (Liu et al., 2019). Photostimulation of A11 DAergic cells reduces trigeminal neuropathic pain through the activation of D_2 receptors in the spinal trigeminal nucleus caudalis; however, an important caveat to this finding is the use of the improper mouse line (DAT-Cre) in this study to appropriately target the DAergic cells of the A11 which are known to be DAT-negative (Koblinger et al., 2014; Liu et al., 2019). Further support to the hypothesis that the A11 descending projections mediate nociception is that spinal

DA receptors inhibit noxious inputs (Jensen and Yaksh, 1984; Puopolo, 2019). Recent work by Piña-Leyva et al. (2020) has suggested that the A11 regulates nociception across spinal cord segments, where the paw withdrawal threshold showed circadian rhythmicity, and this rhythmicity was abolished following 6-OHDA ablation of the A11 region.

In addition, the A11 homolog in zebrafish, the posterior tubercular area (PT), is responsive to mechanosensory stimuli and active preceding locomotor behaviours in a head-fixed setup using a two-photon calcium imaging (Reinig et al., 2017). More specifically, this region's spinally-projecting Ptar and Ptac cells encode the speed and duration of mechanosensory stimuli (Reinig et al., 2017). This study is the only one to date to record the activity of the A11 in a vertebrate model.

1.2.4.4. Sexual Behaviours and Courtship Singing

Given the sexual dimorphism seen in the rodent A11, this region may play a role in sexual behaviours (Pappas et al., 2010). Zebra finches show significant increases in *Fos* levels in the rostral and caudal A11 regions following courtship singing (Bharati and Goodson, 2006). A subsequent study examining pair formation in these birds also demonstrates increased *Fos* levels in the rostral and caudal A11 of male birds, but not in females (Banerjee et al., 2013). In another study of zebra finches, central gray (caudal A11) activity is decreased in female birds who had bonded with a male and were part of a non-aggressive pair (Iwasaki et al., 2014). Work in the male Japanese quail found an increase in the number of cells of the caudal gray (caudal A11) expressing *Fos* in sexually active subjects (Charlier et al., 2005). These studies suggest that the A11 region plays a role in courtship and sexual behaviours in avian models.

Given the sexually related activation of the A11 in humans and birds, it is suggestive of its involvement in sexual functions in mice, forming part of my thesis aims. The courtship singing equivalent in mice consists of ultrasonic vocalizations (USVs) ranging from 30-110 kHz and therefore inaudible to humans (Portfors, 2007; Fonseca et al., 2021). The production of USVs varies across age, sex, and context, and a variety of contexts have been identified as USV-inducing (Whitney et al., 1973; Portfors, 2007). In mice, USVs are most often emitted during non-aversive situations and mating contexts, mouse pups also call and there has been discussion of USVs being involved in territoriality in adult mice (Portfors, 2007; Hammerschmidt et al., 2012; Premoli et al., 2021). Early research suggested only males vocalize during courtship or

mating, but more recent research has shown that females do vocalize during male/female interactions although the majority of calls are produced by males (Premoli et al., 2021).

1.2.4.5. Autonomic Function

The A11's direct spinal connections, along with its proximity to preganglionic neurons and its innervation of the intermediolateral cell column (IML) within the spinal cord, suggest that this nucleus controls autonomic function through its direct DAergic projections to the spinal cord (Lindvall et al., 1983; Holstege et al., 1996; Qu et al., 2006). Early work proposes that the A11's IML innervation acts to suppress sympathetic outflow, and the collateralization of the A11 fibres at the level of the spinal cord suggests that DA modulates both the sympathetic and parasympathetic preganglionic neurons (Holstege et al., 1996). Additionally, work showing the A11 cells being CGRP-positive further suggests this region's role in autonomic function, as CGRP is a potent vasodilator (Orazzo et al., 1993; Russell et al., 2014). In rats, it has been suggested that the A11's connections to the lumbosacral defecation centre may allow this dopaminergic nucleus to modulate defecatory behaviours, another function of the autonomic nervous system (Nakamori et al., 2019). The A11's relationship with the autonomic nervous system has not been fully defined and further work is necessary.

1.2.4.6. Cataplexy

In Doberman dogs, cataplexy (loss of muscle tone related to narcolepsy) was worsened when $D_{2/3}$ agonist drugs are administered into the A11 region, suggesting that A11 DAergic cells, and the DA released from these cells, may counteract cataplexic phenotypes in the hypocretin/orexin-deficient animal model that was used (Okura et al., 2004).

1.3. Dopamine

1.3.1. Dopamine and its Structure and Functions Within the Central Nervous System

Dopamine is produced via a series of enzymatic conversions. With the enzyme tyrosine hydroxylase (TH), tyrosine is converted to L-DOPA (l-3,4-dihydroxyphenylalanine) (Sharples et al., 2014). In turn, L-DOPA, via AADC (amino acid decarboxylase), is converted to DA (Sharples et al., 2014). When DA is released into the synaptic cleft, it is either taken up by DAT and sequestered into synaptic vesicles by VMAT2 or if DA is present within the cytosol, it will

be degraded by monoamine oxidase (MAO) (Meiser et al., 2013). The products of this degradation are hydrogen peroxide and 3,4-dihydroxyphenylacetaldehyde (DOPAL), and DOPAL can be inactivated by alcohol dehydrogenase (ADH) into 3,4-dihydroxyphenylethanol (DOPET), or it can be oxidized by aldehyde dehydrogenase (ALDH) to produce 3,4-dihydroxypheylacetic acid (DOPAC) (Meiser et al., 2013). DOPAL is then usually oxidized to carboxylic acid, and occasionally, DOPAL is reduced to DOPET (Meiser et al., 2013). In addition, DA can be taken up by glial cells where DA is degraded by MAO or catechol-O methyl transferase (COMT) which then produces homovanillic acid (Meiser et al., 2013).

It is well known that DA can act both as a neurotransmitter, by depolarizing or hyperpolarizing the downstream neuron, and as a neuromodulator, by altering synaptic efficiency and neuronal excitability (Nestler, 1994; Kandel et al., 2013; Nadim and Bucher, 2014; Avery and Krichmar, 2017). Dopamine receptors fall under two categories: D_1-like and D_2-like receptors. D_1 and D_5 receptors (D_1-like) are considered excitatory, as they are coupled to G_s G-protein coupled receptors (GPCRs), and activate adenylyl cyclase and increase protein kinase A (PKA) activity (Yamamoto and Vernier, 2011; Sharples et al., 2014). D_2, D_3, and D_4 receptors (D_2-like), are coupled to $G_{i/o}$ GPCRs, and are considered to be inhibitory, as they inhibit adenylyl cyclase and PKA and inhibit voltage-gated calcium channels while activating potassium channels, among other roles in signaling pathways (Yamamoto and Vernier, 2011; Sharples et al., 2014). Dopamine has also been shown to activate trace amine-associated receptors (TAARs), which are found on D cells (monoaminergic neurons able to produce DA and 5-HT in the absence of TH and tryptophan hydroxylase), interneurons, and motoneurons in the spinal cord (Jaeger et al., 1983; Choi, 2018).

In rodent work, DA modulates nociception within the spinal cord in rats (Jensen and Smith, 1982; Megat et al., 2018). There have also been sex differences in DA lumbar spinal cord concentrations in C57BL/6 mice (Pappas et al., 2010).

1.3.2. Dopamine's Role in Locomotor Control

DA contributes to the initiation and termination of locomotion via the canonical basal ganglia circuit through the direct and indirect pathways (Calabresi et al., 2014). Specifically, DA is released from substantia nigra pars compacta terminals onto the GABAergic medium spiny neurons of the dorsal striatum, which then project indirectly onto the mesencephalic locomotor region (Lanciego et al., 2012; Calabresi et al., 2014; Roseberry et al., 2016). Within the basal

ganglia, DA's role at the level of the dorsal striatum is dependent upon the receptors on which it acts, where D_1 receptors are expressed mainly in the direct pathway and facilitate movement by decreasing inhibition of thalamocortical neurons, while D_2 receptors are expressed mainly in the indirect pathway and inhibition of this pathway decreases inhibition of thalamocortical neurons and facilitates movement (Kandel et al., 2013). Both pathways are simultaneously active in certain conditions, which demonstrates that the basal ganglia is involved in the selection of motor actions (Rothwell, 2011).

It is important to note that alternate regions, such as the dopaminergic A11, bypass the basal ganglia to release DA directly onto the spinal cord (see section 1.2.2), implying that the basal ganglia are not the only DAergic effectors of locomotion.

1.3.3. Dopamine and Social Behaviours

Beyond its role in locomotion, DA has been implicated in social behaviours. Work in prairie voles has implicated DA as essential for forming social pairs in males (Aragona et al., 2003). In a fish model, amines including DA modulate aggressive inter-male communication signals (Maler and Ellis, 1987). In mice, the dopaminergic dorsal raphe neuronal activity increases upon reintroduction to social contact following a period of isolation (Matthews et al., 2016). Specifically, these DAergic cells in male mice are active during sociosexual interactions with a female, following social isolation (Cho et al., 2017). Early work investigating dopamine's role in same-sex interactions suggested that $D_{2/3}$ receptors might be involved in defensive behaviours, while more recent work has not only demonstrated increases in extracellular DA and DA transients during same-sex conspecific interactions, but also during copulatory behaviours, in contrast to low extracellular DA concentrations during periods of solitude (Puglisi-Allegra and Cabib, 1997; Robinson et al., 2002). In addition, the administration of amphetamine (a DA activator) show effects on ultrasonic vocalization rates in male mice, but not in females (Wang et al., 2008). In the context of sexual or copulatory behaviour, there is a lack of consensus whether DA acts at the level of the spinal cord (Paredes and Agmo, 2004).

More broadly, dopaminergic ventral tegmental area neurons show increases in activity in response to social interactions and investigation of a novel object, which suggests that DA may also play a role in novelty processing (Gunaydin et al., 2014).

1.3.4. Dopamine and Novelty and Arousal

Dopaminergic populations respond not only to reward and reward prediction, but also to salient, novel stimuli within an environment irrespective of its valence (Avery and Krichmar, 2017). Recent work suggests alternative roles for dopaminergic systems beyond the traditional reward prediction role, based on saliency or uncertainty. The saliency hypothesis suggests that DAergic neurons encode salient, novel stimuli in the environment to discover new actions, rather than using reward prediction error to update a set of defined actions (Avery and Krichmar, 2017). The uncertainty hypothesis suggests that dopaminergic neurons aim to minimize surprise through inference rather than reinforcement learning (Friston et al., 2012). Specific midbrain dopaminergic cell groups of the substantia nigra and ventral tegmental area contribute to novelty processing of objects, not social partners (Tapper and Molas, 2020). Specifically, the peak in DAergic cell activation occurred when exploration of a novel object ended, which the authors suggested could be a reward for successful exploration of a novel object (Tapper and Molas, 2020). Alternatively, dorsal raphe nuclei DAergic cells were not found to be very active when interacting with a novel or familiar object or during locomotor bouts, but showed increased activity when mice were exposed to salient or arousing stimuli such as foot shock, restraint, air puffs, or the consumption of palatable food (Cho et al., 2017).

Overall, it is important to consider that although dopamine plays a significant role in locomotor control, there are a wide variety of behaviours in which DA exerts its effects.

1.4. Approaches to Target A11

Given that the A11 comprises a small population of cells spread rostrocaudally through the posterior hypothalamus, it is important to target this region as specifically as possible. The main targeting method for the A11 which was employed in this thesis is the use of viruses.

1.4.1. Adeno-Associated Viruses

Adeno-associated viruses (AAVs) belong to the Parvoviridae family, which are composed of nonenveloped, small (20 - 26 nm in diameter) viruses with single-stranded DNA genomes (Berns and Giraud, 1996). AAVs are capable of infecting non-dividing cells such as neurons with the assistance of helper viruses like adenovirus or herpesvirus (Berns and Giraud, 1996). There are many serotypes of AAVs produced from a variety of bird and mammal species that have different transduction efficiencies in different cell types (Berns and Giraud, 1996).

However, compared to lentiviruses, AAVs have a limited payload (~9.6 kb), which can restrict their use (Huang and Zeng, 2013). AAVs must be used with an understanding of serotype tissue specificity, virus titer effectiveness, viral preparation, and the potential toxicity of the AAV due to protein accumulation in large quantities (Cearley and Wolfe, 2006; Markakis et al., 2010; Dugué et al., 2012). The transduction efficiency of AAVs is quite high at the injection site, but decreases in efficiency as one moves away from the injection site (Dugué et al., 2012).

AAV9 is a serotype that effectively transduces brain tissue and the AAV9 capsid can undergo axonal transport in the mouse brain and is specific to neurons (Cearley and Wolfe, 2006; Dayton et al., 2012). Additionally, AAV9 efficiently transduces the spinal cord following an intrathecal injection (Gray and Samulski, 2011). The recombinant AAV9 (rAAV9) undergoes both anterograde and retrograde transport in neurons and exhibits slightly increased tropism for the cortex (Haggerty et al., 2020). AAV2/9 (a modified AAV2 with AAV9 characteristics) also shows anterograde transfection at high titers (10^{14} viral particles/mL) (Zingg et al., 2017). Adding promoters to the AAV genome allows increased transduction specificity (Haggerty et al., 2020). For example, Syn (human synapsin 1 gene promoter) is quite commonly used as it targets neuronal populations without the transduction of glial cells (Kügler et al., 2001). This thesis makes use of the EF1a and CAG promoters. The human elongation factor-1a (hEF-1a) and short CMV early enhancer/chicken β actin (sCAG) promoters drive neuronal transduction. There is contradictory work examining the CMV (or CAG) promoter, where CAG is more effective at driving strong gene expression than EF1a or Syn, while another study demonstrated that CMV-promoter constructs show aberrant transcription due to increases in stimulation of neuronal activity through drugs or DREADDs (Damdindorj et al., 2014; Bäck et al., 2019; Nieuwenhuis et al., 2020). Further improvements in the promoter and expression of AAV contents can be accomplished by the addition of the woodchuck hepatitis virus posttranscriptional response element (WPRE), which was utilized within the GCaMP6s construct (Gray and Samulski, 2011).

1.5. Fibre Photometry

Fibre photometry consists of the injection of a fluorescent biosensor (such as the fluorescent calcium sensor GCaMP) and implantation of a fibre optic cannula above the region of interest. During behavioural trials, in vivo measurement of calcium transients via GCaMP within the region of interest is performed by capturing changes in fluorescence and converting these signals into an analog signal which is then digitized (Li et al., 2019). Fibre photometry is

advantageous as it allows for long-term recording from a population of neurons, which can also be cell-type specific depending on the selected virus (Li et al., 2019). It is also technically easier to deploy than *in vivo* electrophysiological methods (Li et al., 2019). The drawback of this technique is the inability to record single-cell activity compared to miniscopes or two-photon microscopy. In addition, some *in vivo* work has shown that long-term expression of genetically encoded calcium indicators over several months can alter cellular physiology (Tian et al., 2009). Despite these shortcomings, fibre photometry remains a tractable option to record activity in deep brain structures such as the A11.

To investigate the innate activity of the A11 region, I used fibre photometry to record neural activity [methods adapted from Li et al. (2017, 2019)]. I made use of a genetically-encoded fluorescent calcium indicator (GCaMP6s) which fluoresces when it binds to calcium ions during an action potential (Nakai et al., 2001; Chen et al., 2013). The targeting of the fibre-optic cannula is important, as the cone of light emitted by the photometry system is relatively small and has a maximal collection range of approximately 300 μm (Pisanello et al., 2019). Using the relative fluorescence of GCaMP6s as a proxy for neural activity allowed me to directly correlate spikes in fluorescence with behaviours to quantify A11 activity during certain locomotor behaviours.

1.6. The Aim of this Thesis

I have highlighted the various roles that the A11 is proposed to serve within the central nervous system. This thesis is focused on the A11's postulated roles in locomotion and sociosexual behaviours. The A11 is in a unique position in rodents as the major direct source of dopamine because of its spinal projections. The literature implicating the A11 in locomotor and sociosexual behaviours suggests that there is important work to be done in elucidating the A11's concurrent activity with these behaviours, as this has not been investigated up to this point.

Further, the work implicating the A11 dopaminergic cell population in locomotor behaviours is important. The A11's direct spinal projections may be the main effectors of this behaviour, which has not yet been explored.

1.6.1. Determine if the A11 is Active During Locomotor and/or Sociosexual Behaviours

Based upon the literature suggesting the A11 plays a role in locomotor behaviours during photostimulation of its dopaminergic population, this thesis will investigate the A11's innate activity during locomotor behaviours to determine a relationship between locomotion and increases in A11 calcium transients recorded via fibre photometry. I hypothesize that the A11 will show increased activity in response to locomotor bouts. In addition, the research in avian subjects suggests that the A11 plays a role in courtship vocalization or sociosexual behaviours. I further hypothesize that the A11 will show increased activity during courtship vocalization and sociosexual behaviours. This work is important because no research to this point has investigated the innate activity levels of the A11 in freely moving vertebrates, and A11 activity recording has been limited to the semi-restrained zebrafish. As such, research has not been able to explore what stimuli or behaviours excite the mammalian A11.

2. CHAPTER 2: The A11's Activity in Response to a Variety of Contexts and Stimuli

Elizabeth M.S. Thurston, Leonardo A. Molina, Van A. Le, Ning Cheng, Cecilia A. Badenhorst, Donovan M. Ashby, Zahra Ghavasieh, Kartikeya Murari, Patrick J. Whelan

Abstract

The A11 nucleus has been previously implicated in a variety of behaviours; however, limited research has investigated this region's innate activity to discern its roles. The A11 region's activity was measured using fibre photometry, and experimental mice were exposed to a variety of contexts and stimuli. Open field data showed that the A11 does not encode velocity but does significantly decrease its activity in response to immobility. In the elevated plus maze, the A11 appeared to increase its activity while out in the open arm, but this was not dependent on the direction of movement within the open arm (towards the end of the open arm or towards the centre). When presented with a novel object, the A11's activity significantly increased from baseline both during investigatory and locomotor behaviours. A11 activity was larger during social behaviours than during asocial behaviours during the presentation of a novel male or female stimulus. The presence of a familiar male stimulus did not significantly increase the A11's activity during goal-directed locomotion but did show an increase during investigatory behaviours. Overall, the heterogeneous A11 population was most responsive to novel social stimuli and responded to investigatory activity, including locomotion. This suggests that the A11 may be responding to novel stimuli by engaging in locomotion.

2.1. INTRODUCTION

The aminergic cell group known as the A11 nucleus has been identified in many species: human, non-human primate, mouse, rat, zebra finch, quail, dog, crocodile, and in zebrafish as a more basal posterior tubercular area (Dahlström and Fuxe, 1964; Skagerberg and Lindvall, 1985; Holstege et al., 2003; Okura et al., 2004; Charlier et al., 2005; Bharati and Goodson, 2006; Qu et al., 2006; Barraud et al., 2010; Lambert et al., 2012; Billings et al., 2020; Fougère et al., 2021). Though this region contains glutamatergic, GABAergic, and dopaminergic neurons, the A11 is best known as the primary source of dopamine in the spinal cord which has been demonstrated in several species including the mouse (Skagerberg et al., 1982; Takada et al., 1988; Takada, 1993; Qu et al., 2006; Lambert et al., 2012; Sharma et al., 2018). This direct connection positions the A11 as important for descending dopaminergic modulation of motor activity within the spinal

cord (Sharples et al., 2014). Previous work in our lab has shown that when the dopaminergic population of cells within the A11 is photostimulated, locomotion is produced, furthering this claim (Koblinger et al., 2018). A significant gap in the field is a lack of knowledge of when the A11 is active during motor behavior. There is currently no extracellular or imaging data published in the freely behaving animal.

The A11 has also been related to sociosexual functions in non-mammalian models. Male zebra finches show increased *fos* protein in the avian rostral and caudal A11 regions following a bout of courtship singing, and the caudal A11 shows decreased activity in females who bonded with a male (Bharati and Goodson, 2006; Iwasaki et al., 2014). In another avian species, males' caudal A11 regions are shown to have increased expression of *fos* when they were sexually active (Charlier et al., 2005). The A11 in mice is sexually dimorphic, which could point to a role in sociosexual functions, and it is important to further investigate its role in a mammalian model (Pappas et al., 2010).

This paper investigates, for the first time, the A11 region's innate activity during a variety of behaviours, both locomotor and sociosexual in nature, using fibre photometry to record calcium transients of this region. Based on previous work in mice and birds, I hypothesized an increase in A11 calcium transients during locomotor behaviours, and during sociosexual behaviours such as the investigation of a novel female. A portion of these results were presented in abstract form (Thurston et al., 2021).

2.2. METHODS

2.2.1. Animals

Male C57BL/6 mice (Charles River Laboratories, Senneville, QC) eight to ten weeks of age at the date of surgery were used. Animal use and surgery were performed in accordance with animal use guidelines set by the University of Calgary Health Science Animal Care Committee (protocol number AC0019-0035). Animals were single-housed following surgery in a 12:12 light:dark cycle (lights on and off at 7 a.m. – 7 p.m.) with *ad libitum* access to water and mouse chow. In total, 21 mice were used. Two mice were excluded before the experiment start point due to surgical recovery complications. Of the 19 remaining mice, nine were excluded from

analysis due to inaccurate targeting of the fibre-optic cannula implantation (see below). For the novelty tests, male and female C57BL/6 mice a minimum of eight weeks old were used.

2.2.2. Experimental Design

2.2.2.1. Surgical Methods

Mice were anaesthetised under isoflurane (4-5% induction, 1% maintenance) via medical-grade oxygen and administered subcutaneous lidocaine (dose: 6 mg/kg, concentration: 20mg/mL) and buprenorphine (dose: 0.05 mg/kg, concentration: 0.03 mg/mL) for analgesia. Mice were then placed in a stereotaxic rig (Stoelting Co., Wood Dale, IL) to secure the head. The scalp was disinfected using betadine and 70% ethanol. The skull was exposed, and a small hole was drilled at the injection coordinates to target the unilateral right A11 nucleus [stereotaxic coordinates: AP 2.30 mm, ML – 0.10 mm, DV -3.3 mm from dura; coordinates adapted from (Koblinger et al., 2018)]. Using a pulled glass pipette, mice were pressure-injected with a GCaMP6s virus, a genetically-encoded calcium indicator (pAAV.CAG.GCaMP6s.WPRE.SV40, Addgene #27056-AAV9, lot #V44841 at a titer of $2.20e^{+13}$ virus molecules per mL) with a Nanoject II (Drummond Scientific Company, Broomall, PA) at a total volume of 124.2 nL (41.4 nL x 3).

A mono fibre-optic cannula (Doric Lenses, Quebec, QC, B280-4401-5, MFC_400/430-0.48_5mm_ MF2.5-FLT) was implanted just above the right A11 (stereotaxic coordinates: AP 2.30 mm, ML -0.10 mm, DV -3.5 mm from dura) and affixed to the skull using a two-step dental cement process [Metabond (K Dental Inc., Markham, ON) and Dentsply (Zahn Canada, Niagara-on-the-Lake, ON)]. Animals were monitored for 48 hours following the surgery and were given a minimum of 28 days to recover and allow for effective viral transfection before the start of experiments. Following the transfection period, mice were habituated to handling daily for five days before the beginning of the experiment and habituated to the photometry fibre and a testing arena for three days before the experiment start.

2.2.2.2. Fibre Photometry System

A Doric Lens System was used: two excitation LEDs (465 nm modulated at 208.616 Hz, and 405 nm modulated at 572.205 Hz; Doric Lenses, Quebec, QC) which were controlled via a 2-channel LED driver (LEDD_2) and fibre photometry console (FPC) running Doric

Neuroscience Studio software. The output signal was demodulated via lock-in amplification. The LEDs were coupled to a Doric filter set (Mini Cube filter set [FMC5_E1(405)_E2(460-490)_F1(500-550)_S]), and the excitation light (465 nm) was delivered to the animal by joining a mono fibre-optic patch cord (DORIC MFP_400/460/900-0.48_2m_FC/MF2.5) to the implanted cannula. The 465 nm LED power was set at 30 µW at the patch cord output (Daviu et al., 2020). The signal was detected using a Digital Optical Power and Energy Meter (PM100D, Thorlabs, Newton, NJ) paired with the S132C Photodiode Power Sensor (Thorlabs, Newton, NJ). The 405 nm LED was adjusted to the same voltage as the 465 nm LED.

2.2.2.3. Behavioural Tests

Open Field Experiment

Mice were connected to the Doric system, and five minutes of fibre photometry recording in the home cage were collected as a baseline. Mice were transferred to an unhabituated open field (OF; 50 x 50 x 50 cm) and left for 10 minutes to roam freely. Behaviour was recorded via top-down video with a Doric Lens camera (BTC_USB3.0, 20 fps) synced to the photometry system. The mice were returned to the home cage for an additional five-minute baseline, after which photometry recording ended. The arena walls and floor were cleaned with 70% ethanol between mice and dried thoroughly prior to the next test. The behavioural videos were processed through TopScan (Clever Sys Inc., Reston, VA) to extract behavioural data. Behavioural and photometry data were imported into a custom MATLAB script, where behaviours were correlated to fluorescence data within the A11 region (Fig. 2).

Elevated Plus Maze

Mice were connected to the Doric system as described previously. Mice were placed into the centre of an unhabituated elevated plus maze (EPM; open arms: 8.5 x 21.5 cm, closed arms: 8.5 x 21.5 x 22 cm, illumination of ~1200 lx at centre) facing a closed arm. Behavioural data were collected via top-down video using the Doric camera, with synchronized fibre photometry data collection. The test was performed for 15 minutes total, with the first and last five mins consisting of the mouse in its home cage while baseline data were collected, while the middle five minutes were completed in the behavioural apparatus. The arena walls and floor were cleaned with 70% ethanol between mice and thoroughly dried before the next test. Behavioural

videos were collected through TopScan to extract behavioural data. The open and closed arms were defined, along with a centre region, to determine spatial occupancy within the maze. The behavioural data were then correlated with fibre photometry data using a custom MATLAB script.

Novelty Tests

The novelty tests consisted of the presentation of a stimulus to a resident mouse in a habituated custom arena (30.48 x 30.48 x 30.48 cm) and the subsequent recording of the vocalizations that ensued using the UltraSoundGate 116H (Avisoft, Berlin, DE) and the accompanying software (recorder USGH 4.3.00, Avisoft, Berlin, DE). The microphone was placed approximately 30 cm above the arena's base, and calls were recorded at a sampling frequency of 250 kHz. The experimental (resident) mouse was habituated to this arena for three days immediately preceding the beginning of experiments, for 15 minutes at a time. On an experimental testing day, the resident was recorded and filmed (top-down video) for five minutes alone before and after the presentation of the stimulus, and the exposure to the stimulus (hand, object, or mouse) lasted for five mins, for a total test duration of 15 minutes. Photometry data were collected throughout this 15-minute test. The video was recorded using an infrared BlackFly camera (Model: BFS-U3-16S2M-CS: 1.6 MP, 226 FPS, Sony IMX273, Mono) with an optical cast infrared longpass filter (Edmund Optics), and Spinnaker SDK (Flir) software. The arena's lighting was custom designed using 940 nm LEDs attached to the roof of the box, along with ambient room lighting. The arena walls and floor were cleaned with 70% ethanol between mice and dried thoroughly before the next test. For the duration of the experiments, the mice were observed from out of view (~1.5 m away) to ensure intruder mice did not begin to chew on the patch cord or fight with the resident mouse.

The five tests which were run were 1) reaching control, 2) novel object, 3) intruder novel male, 4) intruder familiar male, and 5) intruder novel female, in this order. Each test was run on a separate day except for the experiments involving male intruder mice. The order of tests was chosen based on the predicted increase in valence for each stimulus, with a novel female stimulus hypothesized to be the most arousing stimulus. To avoid a confounding variable consisting of a reaching movement into the experimental arena to place or remove a stimulus, a reaching control experiment was the first experiment run in the arena. At both the 5- and 10-

minute mark, the experimenter reached a hand into the arena, touched the centre point of the arena floor, then retracted their hand to habituate the mice. For the novel object test, the object used was 6.3 cm x 7.6 cm x 3.2 cm and was cleaned with ethanol and thoroughly dried between trials. For tests involving an intruder mouse, three different measures of sniffing were collected, but I chose to use the body sniffing measure, which encompassed the more specific anogenital and head sniffing behaviours, for further analysis. For the tests involving intruder males, the same pair of intruder and resident mice were tested for both the novel and familiar male tests, which were run three hours apart on the same day, as the experimental mice retain a memory of this stimulus up to and beyond this time point, as described in Gao et al. (2009). Following the novel female test, the resident photometry mice were perfused after 90 minutes following exposure to the novel female to stain for *c-fos* markers within the A11 region.

2.2.2.4. *Post-hoc* Processing

Perfusion

Mice were transcardially perfused with phosphate-buffered saline, followed by 4% paraformaldehyde (PFA). The head was placed in PFA with the fibre-optic cannula still attached and fixed overnight. The following day, the fibre-optic cannula was removed, and the brain was extracted and post-fixed in PFA for an additional 24 hours, then stored at 4°C and cryopreserved in 30% sucrose.

Immunohistochemistry

Injections and implantations were verified *post-hoc* after brains were sliced coronally using a cryostat (Leica CM1850 UV, Leica Biosystems, Wetzlar, Germany) at 40 μm thickness, and slices were collected in three-series in a well plate to free-float in 1x phosphate-buffered saline (PBS). The slices were immunostained for TH and *c-fos* to localize the A11 region and obtain *c-fos* data. Slices were first washed in 1x PBS at 37°C, then placed in a blocking solution (3% donkey serum in PBS containing 0.5% triton) containing the primary antibodies (Rabbit anti-*c-fos* [1:1000] and Sheep anti-TH [1:500], see table 2.1) overnight at room temperature (RT). Slices were washed in PBS, then placed in PBS containing secondary antibodies (Donkey anti-rabbit-594 [1:500] and Donkey anti-sheep-647 [1:1000], see table 2.2) and incubated for 4 hours at RT. The secondary solution was replaced with DAPI (1:1000 in 1x PBS) for 20 mins,

then washed with 1x PBS at RT before being mounted on Superfrost slides and coverslipped with VectaShield mounting medium (Vector Laboratories Inc, Burlingame, CA, USA).

Table 2.1. Primary antibodies.

Antigen	Lab Code	Commercial Source	Dilution and Incubation Time	Donor Species
TH	AB1542	Millipore	1:500, 24 hrs	Sheep
c-fos	226 003	Synaptic Systems, Göttingen, DE	1:1000, 24 hrs	Rabbit

Table 2.2. Secondary antibodies.

Secondary Antibody	Lab Code	Commercial Source	Dilution
Alexa-594-conjugated donkey anti-rabbit	A21207	Invitrogen	1:500
Alexa-647-conjugated donkey-anti-sheep	A21448	Invitrogen	1:1000
DAPI	D1306	Invitrogen	1:1000

Images were taken on the Slide Scanner (2x/0.08 air, 10x/0.4 air; Olympus VS110-S5, Tokyo, Japan; DAPI excitation [ex] 387/11 nm – emission [em] 440/40 nm; FITC ex 485/20 nm – em 525/30 nm; TRITC ex 560/25 nm – em 607/36 nm; Cy5 ex 650/13 nm – em 684/24 nm) with a camera (Olympus XC10 and XM10). Only mice with on-target GCaMP6s expression and fibre optic implants within 300µm of the A11 were included in behavioural data analysis (Fig. 1 for representative on-target implantation and injection); however, images were acquired from all 19 mice.

2.2.3. Data Analysis

2.2.3.1. Photometry and Behavioural Analysis

Fibre photometry data were processed based upon methods in Martianova et al. (2019) but with small modifications: photobleaching was corrected using an exponential decay function, along with z-score normalization where the mean and standard deviation was calculated from the first five minutes of baseline data (Fig. 2). The area under the curve was normalized by dividing the total area for a given behaviour by its total duration within a test. Behavioural video analysis

was performed by TopScan (Clever Sys Inc., Reston, VA) or custom behavioural categorizations based on work in Le et al. (2021) along with custom MATLAB scripts (scripts available here: https://osf.io/3zxft/?view_only=9ea767be28e94b46ba56b7ee634695cd)

Custom Behavioural Categorization

For the novel object, novel/familiar male and novel female tests, behavioural data were extracted using a custom model expanded upon Le et al. (2021). The current analysis is expanded by extracting behavioural data from multiple mice within a single arena and classifying the data using trained models. The experimental mouse was labelled the resident mouse, while the stimulus mouse was labeled the intruder mouse. For the tests involving an intruder mouse (novel/familiar male and novel female), the following behaviours were extracted: follow, anogenital sniffing, head sniffing, body sniffing, and self-grooming.

To train the model, two observers (one expert, one novice) scored nine randomly selected videos containing the behaviours of interest using BORIS 7.10.2 software (Friard and Gamba, 2016). Then, the dataset was split into a training set containing six videos and a testing set containing three videos (see tables 2.3 and 2.4 for training details). The model was trained with the training set and evaluated based on the testing set. Finally, comparisons between novice-expert and expert-model were obtained on the testing set and were consistent with the literature [i.e. (Lorbach et al., 2018)] and appropriate for our experiments. As such, the data from the model were accepted. Certain behaviours were inferred or modified after output from the model. Body sniffing was generated by combining head sniffing and anogenital sniffing behaviours. Locomotion in the novel object test was calculated by the resident mouse's centre point displacement: a minimum speed of > 60 mm/s and a minimum displacement of 100 mm. Table 2.5 shows the results obtained by the model compared to the novice annotator. The annotation performed by the expert human was considered the ground truth, and F1 was chosen as the performance metric (see Table 2.5).

Table 2.3. Behaviours for the novel and familiar male and novel female tests

Behaviour	**Description**
follow	Resident (R) follows or chases the intruder (I) mouse, attempting to sniff I while I is moving away. If the snout of R comes within a 1 cm distance from any region of I, this counts as sniffing behaviour. The type of sniffing depends on where the snout is directed towards.
anogenital sniffing	Resident directs its snout towards the anogenital region of the intruder (i.e. towards the base of the tail, either touching or within a head-length radius, approximately 2 cm).
head sniffing	Resident directs its snout towards the head of the intruder. This includes the face/nose-to-nose sniffing and sniffing anything above I's shoulders. Behaviours include touching or within an approximate radius of 2 cm radius.
body sniffing	Resident directs its snout towards the body of I. This includes the head sniffing and anogenital sniffing behaviours. Either touching or within a 2 cm radius.
self-grooming	Resident is usually on hindlimbs, grooming its own head or body with forelimbs. Only bouts where R is not in contact with I are included.
locomotion	Resident physically moves or displaces itself from one location to another with a minimum prescribed speed of greater than 60 mm/s and a minimum distance of 100 mm.

Table 2.4. The total time for each behavior in the training set and testing set. Values are in seconds.

	Head Sniffing	**Anogenital Sniffing**	**Follow**	**Approach**	**Self-Grooming**
Training	153.4	342.7	234.5	77.8	55.9
Testing	61.6	152.3	65.4	37.2	16.3

Table 2.5. Comparison of recall, precision, and F1 scores for the human-expert and model-expert configurations.

Metrics	Recall	Precision	F1 Score
Body Sniffing			
Human	0.86	0.98	0.91
Model	0.93	0.91	0.92
Follow			
Human	0.127	0.912	0.223
Model	0.727	0.853	0.756
Approach			
Human	0.455	0.673	0.543
Model	0.421	0.690	0.520
Self-Grooming			
Human	0.460	1.000	0.630
Model	0.460	0.610	0.520

Open Field

In addition to behavioural data being extracted via TopScan, x and y position data were extracted from behavioural videos, and bout-based velocity was calculated using custom MATLAB scripts (see OSF link). From these data, mice were categorized as performing slow or fast locomotor bouts based on individual variation of locomotor speed ("slow": < 3 SD and > 1 SD from individual speed average, "fast": > 3 SD). Locomotor behavior was defined according to TopScan parameters: minimum 100 mm displacement with a minimum speed of 60 mm/s.

Elevated Plus Maze

TopScan was not ideal for collecting locomotor and in-place activity data in the open arms. Given that the mice are locomoting in the EPM's open arms, they are likely locomoting too slowly to be tagged as locomotor bouts, but too quickly to be tagged as in-place activity. As a result, I focused on the spatial occupancy of the EPM as an alternative measure to examine A11 activity in relation to placement in the EPM. There were two options for tracking: nose point and centre point. Investigatory bouts of the open arm were more representative when the nose point was used, and therefore all tracking was used in reference to the nose point.

Novelty Tests

In the novelty tests, ultrasonic vocalizations were only produced during the introduction of a novel female, and therefore analysis of vocalizations for the other novelty tests was not run. For the novel object test, a circumference of 2 cm around the object was defined and when the mouse was facing the object and within this radius, it was considered as exploration or investigation of the object (termed "investigation") (Tapper and Molas, 2020). The behaviour was terminated when the mouse turned away from the object or moved out of the defined radius.

Ultrasonic Vocalization

The ultrasonic vocalization (USV) files were saved as .wav files and were processed using VocalMat [https://github.com/ahof1704/VocalMat, (Fonseca et al., 2021)]. Further *post-hoc* processing was performed within GraphPad Prism 9 and Microsoft Excel. USV-based analysis correlating GCaMP6s signal to vocalization time points or scrambled time points was performed using methods from Chen et al. (2021). In brief, periods of fluorescence ± 75ms at the start of vocalization or randomly selected time points were compared to determine if increased A11 activity was more significantly correlated with the onset of vocalizations than other random time points.

Image Analysis

Following image acquisition, images were processed in IMARIS 8.0 (Oxford Instruments, Abingdon, UK). Within the A11 region of all 19 experimental mice, TH-positive and *c-fos*-positive cells were identified using a threshold based on quality feature and the spots analysis function. A blinded experimenter manually adjusted this threshold to ensure it excluded aberrant signals. TH cells were assigned a cell diameter of 25 pixels and for *c-fos*, a diameter of 10 pixels. A DAPI channel was used to confirm the *c-fos* signal overlapping with the nuclear stain. Then, after machine learning was enabled, thresholded images were used to create a mask to calculate the total number of TH-positive cells and TH-positive cells containing *c-fos* expression. Results were also manually checked by the blinded experimenter. I then determined the proportion of DAergic A11 cells that were active during the novel female test.

2.2.3.2. Statistical Analysis

Values are reported as mean ± standard deviation unless otherwise stated. Statistical analyses were performed using GraphPad Prism 9. Data were tested for normality (D'Agostino-Pearson test) and if normal, a paired two-tailed t-test or a one-sample two-tailed t-test was used. Otherwise, a Wilcoxon matched-pairs signed rank test was used. Simple linear regressions and runs tests or exponential decay curves were fit to bout-based maximal fluorescence data. Alpha was set to 0.05. In a few cases, mice were excluded from a specific test for analysis due to methodological errors.

2.3. RESULTS

Only male mice were used because of the statistical power required, though the inclusion of female mice in the future is of great importance. The area under the curve (AUC) data represent the magnitude of fluorescence, while maximal fluorescence represents the maximal fluorescence achieved during a specific behaviour. Start and stop graphs are helpful to determine how the A11's activity changes about the onset or offset of different behaviours. The measured behaviours for each behavioural test and their within-trial frequency across individual mice are presented in Table 2.6. In certain analyses, sample sizes are smaller than the total number of mice used, because of either exclusion of individual mice due to recording issues, or because the analyzed behaviours were not performed by certain subjects.

Table 2.6. Range of bouts for defined behaviours.

Test	Measured Behaviour	Range (min - max)
Open Field	No Movement	3 - 29
	Locomotion	43 - 103
	Fast	8 - 22
	Slow	0 - 30
Elevated Plus Maze	Nose in Closed Arms	11 - 22
	Nose in Open Arms	0 - 16
Novel Object	Investigation	5 - 46
	Locomotion	7 - 55
Novel Female	Body Sniffing	32 - 55
	Follow	2 - 16
	Self-Grooming	0 - 7
USV	Vocalization	349 - 1746
Novel Male	Body Sniffing	28 - 54
	Follow	1 - 12
	Self-Grooming	0 - 9
Familiar Male	Body Sniffing	25 - 60
	Follow	0 - 9
	Self-Grooming	0 - 6

2.3.1. Open Field

The first question I asked was whether locomotion itself could activate the A11 region, implicating it as a motor command centre. The animal was placed in an unhabituated open field (Fig. 2.3A) to measure locomotor activity. Figure 2.3B illustrates the A11's activity during periods of activity and inactivity, where there are clear periods of depressed A11 activity during no movement, compared to locomotion. There was a significant difference between locomotor (-0.17 ± 0.65, $n = 9$) and no movement (-1.15 ± 0.78, $n = 9$) behaviours, as measured by the AUC (Wilcoxon matched-pairs signed rank test, $p = 0.0039$, $W = 45.00$, Fig. 2.3C). However, when I also tested each of these data against a baseline value of 0.00, a one-sample t-test found significant differences for no movement ($p = 0.0022$, $t = 4.422$, $df = 8$), but not for locomotion ($p = 0.4655$, $t = 0.7664$, $df = 8$). In addition, a significant difference was found for maximal fluorescence data between locomotion ($n = 9$, 0.70 ± 1.84) and no movement (-0.57 ± 0.89, $n = 9$) behaviours (Wilcoxon matched-pairs signed rank test, $p = 0.0078$, $W = 43$, Fig. 2.3D), suggesting that the A11 is more maximally active in response to locomotor behaviours. In addition, the average z-score ($\pm$ 5 seconds from behaviour onset) was graphed, which shows a slight decrease in A11 fluorescence at the onset of no movement, which is not present with the

onset of locomotion (Fig. 2.3E). In summary, OF results showed no changes from baseline when the animal was locomoting. However, velocity could have been a factor. Thus, for the OF velocity-based data, the AUC data were analyzed to determine differences in A11 activity during fast (-0.22 ± 0.57, n = 9) and slow (-1.63 ± 0.76, n = 8) locomotor bouts, and there was no significant difference found (Wilcoxon matched-pairs signed rank test, $p = 0.3828$, $W = -14.00$, Fig. 2.3G). The maximal fluorescence data showed no significant difference (Wilcoxon matched-pairs signed rank test, $p = 0.0547$, $W = -28$) between fast (-0.07 ± 0.63, n = 9) and slow (0.078 ± 0.91, n = 8) locomotor bouts (Fig. 2.3H). The average trace at the onset of either a slow or fast locomotor bout look similar (Fig. 2.3I). In summary, A11 activity was not correlated to locomotion as hypothesized. Given that my hypothesis was not supported, I decided to include a battery of behavioural tests to test A11 activity in a broader set of contexts.

2.3.2. Elevated Plus Maze

I first examined the EPM, which provides a measure of anxiety and is a robust, validated test (Fig. 2.4A). Specifically, there is a difference in exploring the closed and open arms based on emotional state, which could translate into A11 activation patterns within the maze.

Figure 2.4B shows the A11's activity in a sample trace, where the differences in activity between the open and closed arms seem to be slightly different. When examining the AUC, there was a significant difference in the open (0.75 ± 0.86, n = 9) compared to closed (-0.61 ± 0.94, n = 9) arms (paired t-test, $p < 0.0001$, $t = 8.113$, $df = 8$, Fig. 2.4C). A one-sample t-test found that the AUC for the closed arm was not significantly different from baseline ($p = 0.0877$, $t = 1.944$, $df = 8$). There was a significant difference in maximal fluorescence values in the open (1.18 ± 0.97, n = 9) compared to closed arms (0.96 ± 0.89, n = 9) (paired t-test, $p = 0.0105$, $t = 3.319$, $df = 8$, Fig. 2.4D). This suggests that the A11 is more active in the open arms reflecting a less anxious state.

I then considered whether the A11's activity differed when the mouse was traveling towards the end of the open arm (distal movement) compared to when it was returning towards the centre (proximal movement). The AUC data showed that there was no significant difference between distal (1.12 ± 2.15, n = 6) and proximal (1.12 ± 1.61, n = 6) movements (Wilcoxon matched-pairs signed rank test, $p > 0.999$, $W = 1$, Fig. 2.4E). Similar conclusions were found for

maximal fluorescence values: proximal (1.67 ± 1.76, n = 6), distal (1.71 ± 2.07, n = 6), comparison Wilcoxon matched-pairs signed rank test, p = 0.5625, W = 7, Fig. 2.4F).

2.3.3. Novelty Tests

Given that the A11 seemed to respond to the exploration of the open arm of the EPM, but did not respond strongly to locomotor bouts in the open field, I chose to focus on the activity of the A11 in interactions with novel objects and social interactions with male and female mice to determine if differences in context, novelty, and stimulus type would elicit differences in activity in the A11.

2.3.3.1. Novel Object

I first introduced a novel object as a control for the later social stimuli tests (Fig. 2.5A). The sample trace (Fig. 2.5B) shows that the A11's activity seems to increase during the investigation of a novel object, but that locomotor behaviours are often paired with investigatory behaviours. I tested whether the A11's activity was significantly different from baseline (value of 0.00) for investigation (1.87 ± 0.86, n = 10) and locomotion (1.13 ± 0.79, n = 10). I found significant differences both for investigation (one-sample t-test, $p < 0.0001$, $t = 6.888$, $df = 9$) and locomotor behaviours (one-sample t-test, $p = 0.0014$, $t = 4.554$, $df = 9$; Fig. 2.5C). When I examined the maximal fluorescence data, there was a significant difference from baseline for both investigation (2.07 ± 0.85, n = 10; one-sample t-test, $p < 0.0001$, $t = 7.685$, $df = 9$) and locomotor behaviours (1.37 ± 0.82, n = 10; one-sample t-test, $p = 0.0005$, $t = 5.306$, $df = 9$; Fig. 2.5D). Examining the change in A11 activity at the offset of investigation and locomotor behaviours (Fig. 2.5E), there is a peak in A11 fluorescence during investigation compared to locomotor behaviour. In summary, there is an overall change in the level of fluorescence during both behaviours, but only during investigation was there a time-locked increase in A11 activity.

To further test the hypothesis that the A11 activity is associated with novelty, I chose to expose the resident mice to novel social stimuli to determine whether the type of stimulus may alter the A11's response differently.

2.3.3.2. Novel Female

I presented an intruder novel female stimulus to the resident male mice (Fig. 2.6A) to elicit ultrasonic vocalizations and determine if a novel sociosexual partner would elicit similar increases in A11 activity as seen in the novel object test. Figure 6B shows that the A11's activity is quite low during self-grooming compared to body sniffing. The AUC data showed that there was a significant difference between self-grooming (-0.17 ± 0.40, n = 8) and body sniffing (1.42 ± 0.71, n = 10; paired t-test, p <0.0018, t = 4.895, df = 7; Fig. 2.6C). There was also a significant difference between self-grooming and follow (1.33 ± 0.82, n = 10; Wilcoxon matched-pairs signed rank test, p = 0.0078, W = 36; Fig. 2.6D). For maximal fluorescence data, there was a significant difference between self-grooming (0.32 ± 0.34, n = 8) and body sniffing (1.61 ± 0.64, n = 10; paired t-test, p < 0.0025, t = 4.607, df = 7, Fig. 2.6E), and a significant difference comparing self-grooming and follow (1.49 ± 1.04, n = 10; Wilcoxon matched-pairs signed rank test, p = 0.0078, W = 36, Fig. 2.6F). This suggests that the A11 in a social test shows decreased activity when engaging in asocial behaviours (self-grooming), while body sniffing which is an investigatory behaviour, increases the A11's activity. In addition, the goal-directed follow behaviour also elicits a large increase in A11 activity.

<u>Ultrasonic Vocalizations</u>

Given the A11's sexual dimorphism and role in sociosexual behaviours in birds, I chose to determine if the A11's activity increased during courtship vocalizations. Ultrasonic vocalizations were recorded during the novel female test (sample trace in Fig. 2.7A) and fluorescence data for scrambled (0.89 ± 0.62, n = 10) and vocalization (1.36 ± 0.73, n = 10) time points were found to be significantly different (paired t-test, p = 0.0003, t = 5.640, df = 9, Fig. 2.7B), suggesting that the A11 encodes ultrasonic vocalizations, a first in the mouse model.

2.3.3.3. Novel Male

As a result of the A11's increased activity in response to a novel female stimulus, I chose to present a novel male (Fig. 2.8A) to determine if A11 activity would be different in response to a conspecific of the same sex. A sample trace (Fig. 2.8B) does not show obvious trends; however, I tested AUC data to determine if self-grooming differed significantly from the two behaviours. AUC data showed a significant difference between self-grooming (0.10 ± 0.77,

n = 9) and body sniffing (1.85 ± 0.95, n = 10; paired t-test, p = 0.0017, t = 4.635, df = 8, Fig. 2.8C). A significant difference was also found for AUC data for self-grooming and follow (1.89 ± 0.87, n = 10; unpaired t-test, p = 0.0023, t = 4.382, df = 8, Fig. 2.8D). For maximal fluorescence data, there were significant differences when comparing self-grooming (0.81 ± 0.72, n = 9) and body sniffing (2.00 ± 0.86, n = 10; paired t-test, p = 0.0047, t = 3.881, df = 8, Fig. 2.8E), as well as self-grooming and follow (2.09 ± 0.94, n = 10; paired t-test, p = 0.0090, t = 3.427, df = 8, Fig. 2.8F). These results suggest that the A11 increases its activity like the presentation of a novel female: increased activity related to the investigation of the stimulus (follow, body sniffing) compared to asocial self-grooming, which does not involve the stimulus.

2.3.3.4. Familiar Male

I then tested whether the presentation of a familiar social stimulus would change the A11's activity in response to novelty. I tested whether AUC was different between self-grooming and two behaviours. A significant difference was found comparing self-grooming (0.29 ± 1.49, n = 9) and body sniffing (1.05 ± 0.66, n = 10; Wilcoxon matched-pairs signed rank test, p = 0.1641, W = 25, Fig. 2.9C). No significant difference between self-grooming and follow (1.03 ± 1.02, n = 9) was found (Wilcoxon matched-pairs signed rank test, p = 0.1484, W = 22, Fig. 2.9D). For maximal fluorescence, no significant difference was found between self-grooming (0.85 ± 1.58, n = 9) and body sniffing (1.26 ± 0.67, n =10; Wilcoxon matched-pairs signed rank test, p = 0.3594, W = 17, Fig. 2.9E), as well as no significant difference between self-grooming and follow behaviours (1.24 ± 0.99, n = 9; Wilcoxon matched-pairs signed rank test, p = 0.5469, W = 10, Fig. 2.9F). These data illustrate that when compared to asocial self-grooming, the A11 does increase its activity during the investigation of a familiar stimulus but does not change its activity during goal-directed locomotion. The lack of significance in maximal fluorescence data suggests that the A11's maximal response is similar between investigatory and asocial behaviours.

2.3.3.5. Reaching Control

In this test, I was only tracking A11 activity in response to the reaching stimulus [AUC (n = 10, 1.42 ± 1.04), max (n = 10, 1.67 ± 1.05); see Appendix 1]. A one-sample t-test found that the A11's response to reaching was significantly increased from baseline (0.00) for both AUC (p = 0.0019, t = 4.316, df = 9) and maximal fluorescence data (p = 0.0007, t = 5.029, df = 9).

2.3.4. Comparison Analysis

I next chose to examine whether the relative novelty or sex of the intruder increased A11 activity (Fig. 2.10). I chose body sniffing as the social behaviour to compare between tests because it encompasses more specific types of investigatory behaviour (head sniffing, anogenital sniffing).

Male Versus Female

The A11 does not change its relative activation between the presentation of a conspecific of the same or opposite sex. There was no significant difference in AUC data for body sniffing of a novel male (1.85 ± 0.95, n = 10) or novel female (1.42 ± 0.71, n =10) (paired t-test, $p = 0.0641$, $t = 2.110$, $df = 9$; Fig. 2.10A) despite average time spent body sniffing being significantly different between the novel male (100.20 ± 24.77 s) and novel female (137.30 ± 23.60 s) stimuli (paired t-test, $p = 0.0035$, $t = 3.922$, $df = 9$; Fig. 2.10B).

Novel Versus Familiar Male

Novelty of a male mouse stimulus does affect the A11's activity: a significant difference in body sniffing AUC data was found when comparing a novel (1.85 ± 0.95, n = 10) or familiar male (1.05 ± 0.66, n = 10) stimulus (paired t-test, $p = 0.0087$, $t = 3.334$, $df = 9$; Fig. 2.10C). Average time spent body sniffing was not significantly different between the novel male (100.20 ± 24.77 s) and familiar male (103.40 ± 22.18 s) stimuli (paired t-test, $p = 0.6643$, $t = 0.4486$, $df = 9$; Fig. 2.10D).

2.3.5. Decay Analysis

If novelty were of importance, I would predict a decay following repeated exposure to the novel object or mouse, which would be most apparent in the maximum fluorescent response. Therefore, group mean maximal fluorescence values were compared across the first ten bouts of investigatory behaviour in each novelty test.

Novel Object

An exponential decay curve was fit to the average data ($Y0 = 4.25$, plateau = 2.04, tau = 2.55; Fig. 2.11A). The individual-level data showed that eight of ten subjects' maximal

fluorescence data fit a simple linear regression (six of eight showed a negative slope). In contrast, two of ten individuals showed a significant deviation from linearity following a runs test and were better fit using an exponential decay curve. In all mice, I observed a decrease in fluorescence with time.

Novel Female

An exponential decay curve was fit to the average data (Y0 = 6.97, plateau = 1.76, tau = 2.29; Fig. 2.11B). At the individual level, six of ten subjects' maximal fluorescence data fit a simple linear regression with negative slopes. The remaining four showed a significant deviation from linearity following a runs test. They were better fit with an exponential decay curve (see appendix 2 for individual subject data).

Novel Male

An exponential decay curve was fit to the average data (Y0 = 7.12, plateau = 2.22, tau = 2.62; Fig 2.11C). The individual maximal fluorescence data for eight of ten subjects fit a simple linear regression with negative slopes. The remaining two subjects significantly deviated from linearity following a runs test and were fit with an exponential decay curve.

Familiar Male

An exponential decay curve was fit to the average data (Y0 = 7.272, plateau = 1.416, tau = 2.353; Fig. 2.11D). The individual maximal fluorescence data for four of ten subjects fit a simple linear regression, demonstrating negative slopes. The remaining six of ten subjects significantly deviated from linearity after a runs test and better fit an exponential decay curve.

Overall, we found evidence for decay with stimulus presentation in all tests we conducted, with the least decay observed for novel objects.

2.3.6. Dopaminergic Cell Activity Via Immunohistochemical Methods

When the A11 region was stained for TH and *c-fos* following the presentation of a novel female, I found that approximately 6% of TH-positive cells were *c-fos*-positive (Fig. 2.12), suggesting that most active cells were not DAergic.

2.4. DISCUSSION

The A11 comprises a heterogeneous cell population, and the methods I used in this experiment were essential for recording activity from the entirety of this population. In the first attempt to record in a freely moving vertebrate, I set out to determine if the A11 region was active during locomotor behaviours. I found that the A11's activity increased during the investigation of novel stimuli, and goal-directed locomotion was also associated with increased regional activity. This adds to the A11 literature as this is the first time that response to novelty and investigatory behaviours have been ascribed to this region.

In an unhabituated open field, the A11 did not respond to locomotor bouts but did dampen its activity during bouts of no movement. In addition, the A11 did not appear to encode velocity. This was counter to our original hypothesis where I expected an increase in population-level activity based on Koblinger et al. (2018). This suggests that the A11 is not acting as a motor command centre (which would show increases in activity with any locomotor activity) but instead may be playing a modulatory role. In addition, the A11 population does not seem to be responding in a fashion similar to other brainstem locomotor centres, such as the medullary reticular formation, where regional activity is related to velocity (Chang et al., 2021). The delay in locomotor behaviours observed in Koblinger et al. (2018) during photostimulation also demonstrates that the A11 is not modulating locomotion through the mesencephalic locomotor region, as the direct stimulation of this region produces locomotion within 700 ms (Chang et al., 2021). Given that the A11 region's activity did not appear to be associated with locomotor behaviours in the unhabituated open field, I chose to place the experimental mice into a broader set of experimental paradigms to explore what contexts or stimuli might elicit a more robust increase in A11 activity.

In the elevated plus maze, I found that the A11's activity was increased when the animals were in the open arms as opposed to the closed arms of the arena. Though both the elevated plus maze and open field offer novel environments to explore, the difference in A11 activity could be explained by locomotor behaviours in the elevated plus maze being more goal-directed than in the open field, where there are discrete spatial regions in the elevated plus maze compared to the open field arena. When I examined if the A11's activity was dependent on whether the animal was moving out towards the open arms or moving back towards the safety of the closed arms, I

did not see any significant difference, suggesting that the A11 might be more responsive to context-dependent exploration, decreased anxiety, or arousal. Therefore, I chose to present novel stimuli as the next paradigm to determine if the A11 responded to decreased anxiety and exploration in the elevated plus maze.

When I placed the experimental mice into a habituated arena and presented them with a novel object, I found that A11 activity increased compared to baseline during both investigation and locomotor behaviours. The novel stimulus was placed in an arena where the experimental mice were habituated while the open field was unhabituated. Therefore, the locomotor behaviours within these two tests were different. The mice engaged in exploratory locomotion in the open field but more goal-directed movement in the novel object test. The peak GCaMP signal occurred at the offset of investigatory behaviours. Given that the A11 significantly increased its activity during locomotor bouts in a specific context, but not during all locomotor behaviours in all contexts, I suggest that this region responds to goal-directed locomotor behaviours in specific investigatory contexts. A significant body of work implicates dopaminergic regions in novelty or investigatory behaviours: work in the nucleus accumbens shows that the dopaminergic population releases dopamine to reinforce “advantageous behavioural outcomes” in a fear conditioning setup (Oleson et al., 2012).

Further work in the striatum found that dopaminergic cells’ responses peaked at the retreat from a novel object rather than upon approach of the novel object and that, similar to my work, the GCaMP signal was not related to velocity or onset of locomotor behaviours (Menegas et al., 2018). They also found that the cells showed increased GCaMP fluorescence with a novel stimulus than a familiar stimulus and that the investigatory bouts involved quick retreat behaviours (Menegas et al., 2018). In rats, 6-OHDA into the anterolateral hypothalamus led to decreased exploratory locomotion (due to loss of DA in bed nucleus of the stria terminalis, lateral septal nucleus, and nucleus accumbens, all of which are A11 afferents), and when treated with apomorphine, only rescued exploratory locomotion in response to a novel object, not familiar (Fink and Smith, 1980). These studies illustrate that DA and the hypothalamus have been implicated in investigation or goal-directed locomotor behaviours targeted towards novel inanimate stimuli suggesting that the A11, being both DAergic and a subregion of the hypothalamus, might play similar roles related to novelty. It may also point to exploratory

locomotion directed towards novel stimuli being governed by a different circuit than towards familiar stimuli. In considering that the A11 is a heterogeneous cell population, it is also worth noting that other hypothalamic regions with glutamatergic and GABAergic cells are involved in motivated behaviours; in the lateral hypothalamus-ventral tegmental area circuit, GABAergic cells have been shown to promote motivated behaviours (such as feeding, social interaction, or approach/avoidance) (Nieh et al., 2016). On the other hand, glutamatergic cells have been shown to suppress those behaviours (Nieh et al., 2016). The photostimulation of the GABAergic cells of the A11's neighbouring medial zona incerta produced increased interaction with novel, but not familiar, objects and increased investigation of intruder social partners (Ahmadlou et al., 2021). In contrast, photoinhibition of these same populations produced opposing behavioural effects (Ahmadlou et al., 2021). Further work in the lateral hypothalamus has shown cell-type-specific responses to novel objects where melanin-concentrating hormone-positive neurons showed increased activity during investigation, while hypocretin/orexin neurons did not show changes in the activity (Kosse and Burdakov, 2019).

During the presentation of the novel male, I found a significant increase in A11 fluorescence during body sniffing compared to the asocial self-grooming behaviour. In addition, targeted locomotion ("follow") towards the intruder mouse showed an accompanying elevation of A11 activity. This suggests that the A11 responds to the novel social stimulus by engaging in goal-directed locomotion. It is also well-known that novelty increases attention and alertness, and is a component of salience (Tapper and Molas, 2020).

When the same male stimulus was presented again as a familiar male, only the body sniffing behaviour was significantly different from self-grooming behaviour. The follow behaviour targeted towards the intruder mouse was not significantly different from self-grooming. These results suggest that the A11's goal-directed locomotion during social investigation is modulated by novelty. When I directly compare the AUC for body sniffing between the novel and familiar male, there is a significant decrease in A11 activity.

When I presented a novel female stimulus, the A11 increased its activity during social behaviours and goal-directed locomotion compared to the asocial self-grooming behaviour. When I compared the A11's activity between a novel female and male mouse stimulus, the AUC

data were not significantly different during body sniffing. In addition, when I examine the maximal fluorescence achieved at the level of the A11 in response to early and later bouts of approach to a novel object, I see a decay in the maximal fluorescence, again suggesting that the A11's activity is dampening in response to increased familiarity of the object. Other DAergic regions (caudate putamen, olfactory tubercule, and nucleus accumbens shell) have shown decreased responses once presented with a previously novel but now familiar social stimulus (Robinson et al., 2002). I also demonstrate that the decay in maximal fluorescence is steeper when considering social stimuli. Rodents prefer social stimuli over inanimate stimuli, suggesting that this preference results from different circuits modulating the two (Gunaydin et al., 2014; Tapper and Molas, 2020).

My data suggest that the A11 increases its activity during periods of goal-directed locomotion, explicitly targeted towards novel objects or social stimuli. I suggest that, given the A11's attenuated response during goal-directed movement towards the familiar male stimulus, a novel stimulus (whether it be social or inanimate) excites the A11 and encourages the production of goal-directed investigatory behaviours. Previous research has shown that some of the afferent projections onto the A11 (the perirhinal cortex, hippocampus, and amygdala) respond to novelty, and the locus coeruleus, a known A11 efferent, is also involved in novelty processing which could formulate a circuit through which the A11 might be involved in the response to novelty (Maeda et al., 1991; Beckford, 2008; Schomaker and Meeter, 2015; Koblinger, 2017). Results seen in Koblinger et al. (2018) where the A11 produced locomotor behaviours during photostimulation in an open field could be a result of the artificial activation of a circuit that, in a natural activation state, is correlated with goal-directed locomotion but when artificially stimulated, produces the output behaviour without the requirement of a novel stimulus. An alternative explanation for the elevation of A11 activity in response to novel stimuli could be its role in nociception. Given that the A11 is known to project to the periaqueductal gray and dorsal horn of the spinal cord, it is possible that it could be gating pain in the face of novel, potentially threatening stimuli to ensure escape is possible. More broadly, perhaps the A11 increases general arousal to prime the mouse to respond to novel stimuli, as a result of its efferent connection with the locus coeruleus and the A11's potential autonomic functions (Skagerberg et al., 1982). Conversely, the A11's role in nociception at the level of the spinal cord could be working directly to suppress pain while also promoting investigation of novel stimuli.

When I examined whether the A11's activity increased in response to ultrasonic vocalizations during the novel female test, I detected a significant increase in calcium transients. This supports the hypothesis that the A11 is involved in sociosexual behaviours like birds. Work in zebra finches showed that male finches had increased activity (*Fos*) following courtship singing to a female (Bharati and Goodson, 2006). As reported by Chen et al. (2021), I cannot attribute all the USVs to the male mouse as females also call to males, and approximately 30% of calls produced by a male-female dyad are produced by the female (Premoli et al., 2021). The GCaMP6s construct that I employed in this experiment did not allow me to further investigate the correlation between A11 activity and specific types of calls or any more specific alterations in A11 activity according to USVs given its changes in fluorescence (~200 ms peak time) are slower than the production of a single USV syllable (on average, 35 ms) (Chen et al., 2013; Weiner et al., 2016). In addition, the hypothesis that the A11 is involved in sociosexual behaviours is supported by the sexual dimorphism displayed by the A11. More TH-positive cells and spinal DA released in males suggest sex-biased functionality (Pappas et al., 2011). My results showing that only 6% of TH-positive cells also expressed *c-fos* following the novel female test do not support the idea that the intruder mouse significantly activated these DAergic cells, which could partly explain species differences. My work suggests that the A11 is responding to a novel social stimulus and the vocalizations that accompany the presentation of a novel female stimulus.

These methods allowed me to collect activity from the entirety of the heterogeneous A11 region, while the optogenetic stimulation paradigm by Koblinger et al. (2018) specifically targeted DAergic cells of this nucleus. My approach provides important data regarding the A11's activity as a whole (made up of peptidergic, glutamatergic, GABAergic, and DAergic cells), rather than simply focusing on the A11's DAergic cells which are spread throughout the length of the nucleus (Orazzo et al., 1993; Kawano et al., 2006; Fougère et al., 2021; Yamaguchi et al., 2021). The sparseness of the DAergic cells in the region would have likely produced only minor changes in fluorescence, of which only a small proportion would have had their fluorescence captured by the fibre-optic cannula in the current setup. In addition, the *c-fos* data collected following the novel female test suggests that the A11's non-DAergic cells are more active than the DAergic cells. Though I cannot be sure that the non-DAergic cells are active in the other

contexts, these cell types may offer more insight into A11 activity patterns in different contexts than the DAergic population.

This work is not without limitations. The A11 is a long nucleus, and the mid- to caudal A11 is more easily targeted than the rostral A11; therefore, most recorded mice did not include activity from the rostral A11. There are differences in A11 cell type heterogeneity across the rostrocaudal extent of the A11 (Abdallah et al., 2015; Yamaguchi et al., 2021), which would not have been represented in this work. In addition, this work only used male mice, and the sexual dimorphism of the A11 indicates that the activity of this region may differ by sex.

Future work could further examine several aspects of the current research. Firstly, the inclusion of experimental female mice in future cohorts is important. Additionally, immunohistochemical results have indicated that the non-DAergic cell population of the A11 is more numerous than the DAergic cell population and appears to contribute to the photometry signal in response to a novel female stimulus, as seen in the *c-fos* stain results. It would be necessary first to confirm the presence of glutamatergic cells in the adult male, building off results from Fougère et al. (2021), likely through an *in situ* hybridization approach. Future experiments could use a VGLUT2-Cre mouse line or GAD67-Cre mouse line and a faster GCaMP variant to investigate cell-type-specific activity in response to novel social and asocial stimuli and the effect of novelty on A11 activity. Though a TH-Cre mouse line would target the A11 DAergic cells appropriately, it would be recording from a very small subset of cells in this region, and the actual activity pattern may not be captured. Alternatively, a miniscope approach or extracellular recordings from this region would allow for single-cell activity measurements.

My work showed that the A11 responds most strongly to novel stimuli and associated investigatory behaviours. It also revealed that the A11 responds to courtship ultrasonic vocalizations and shows depressed activity during asocial self-grooming or during periods of immobility in the open field. In contrast, but it does not respond strongly to locomotion in the open field. Overall, this sets the stage for future experiments which may explore the A11's newfound role in novelty, ultrasonic vocalizations, and goal-directed locomotion.

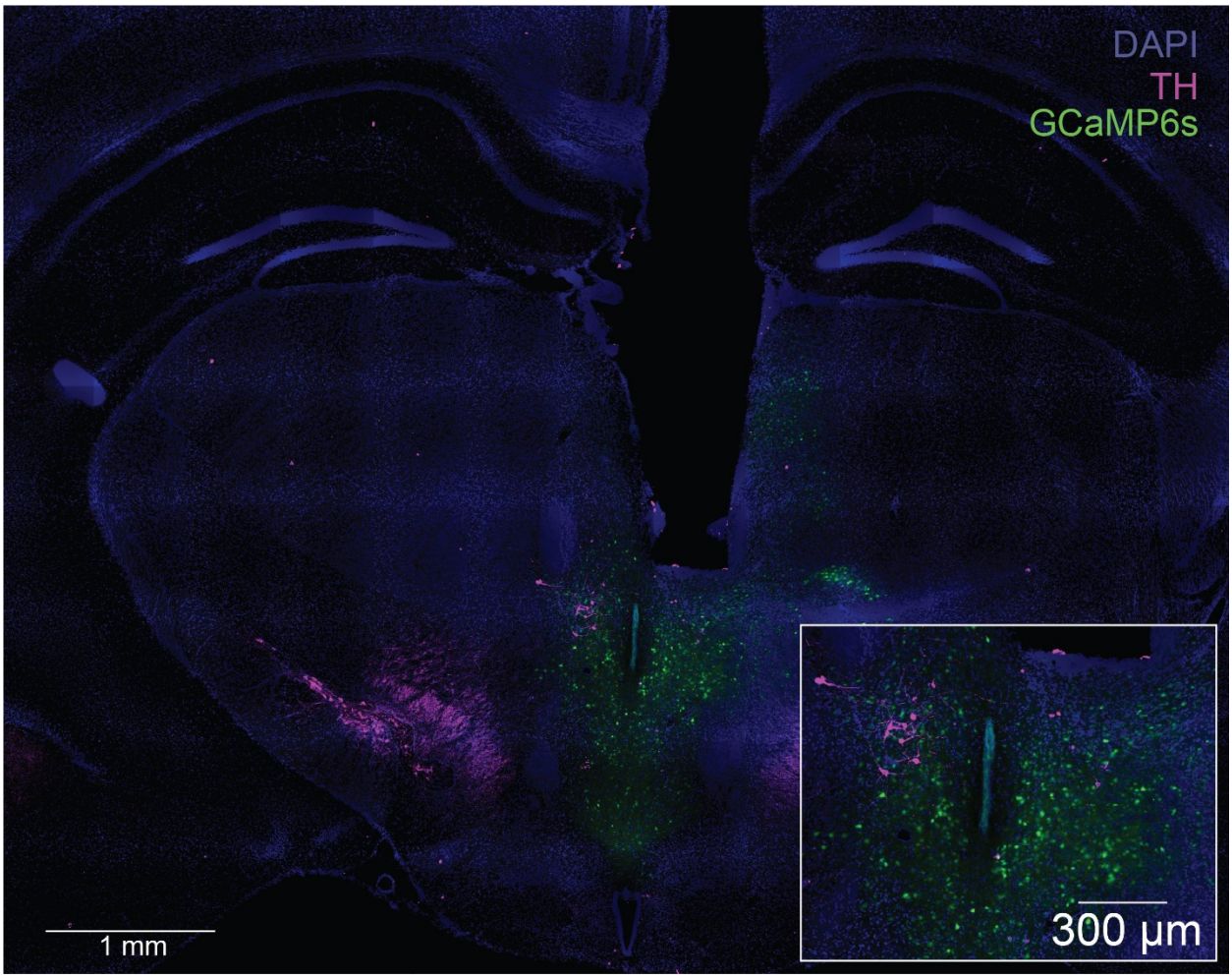

Figure 2.1. Sample image of the A11 successfully being targeted by a fibre-optic cannula. The cannula tract is visible targeting the mid-A11 region. GCaMP6s is visible in green, DAPI in blue, and TH in magenta. The inset shows the A11 region in greater detail.

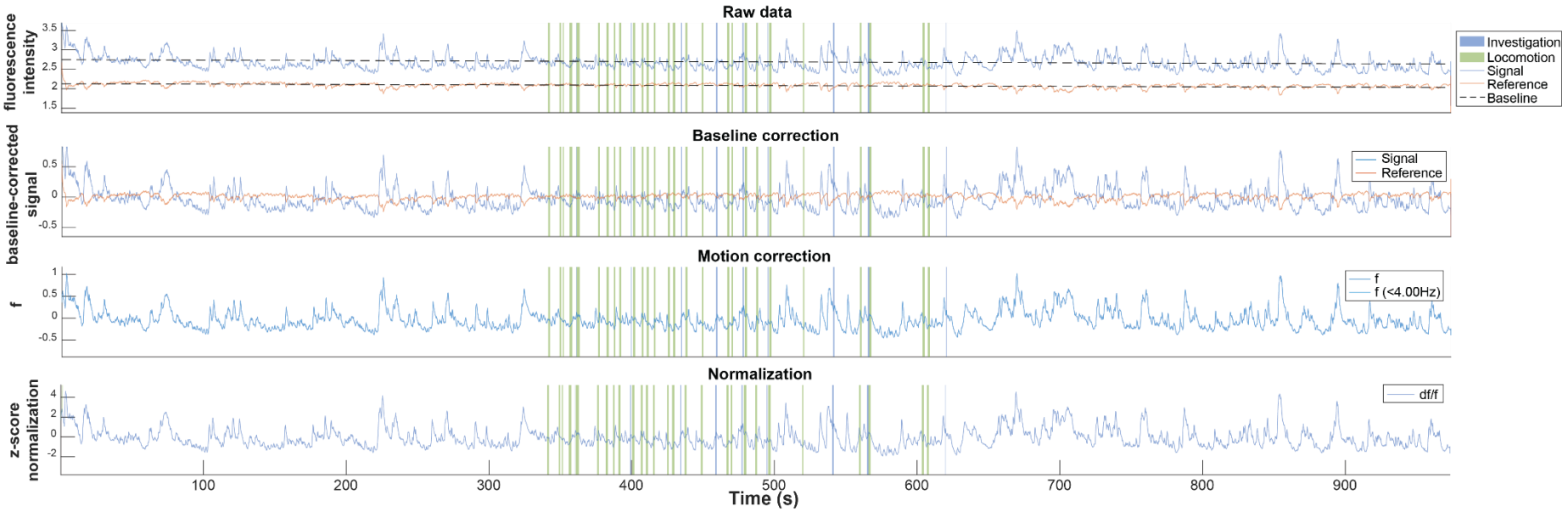

Figure 2.2. Sample of the custom MATLAB fiber photometry analysis script's steps. Raw 405 nm and 465 nm signals are present in the raw data panel. In the baseline correction panel, the two channels are fit to an exponential decay curve. In the motion correction panel, the 405 nm channel is subtracted from the 465 nm channel to correct for motion artifacts in the signal channel. Once the z-score calculation is applied to the first 300 seconds in the normalized panel, the new z-score data are graphed. Steps are based upon data analysis steps outlined in Martianova et al. (2019).

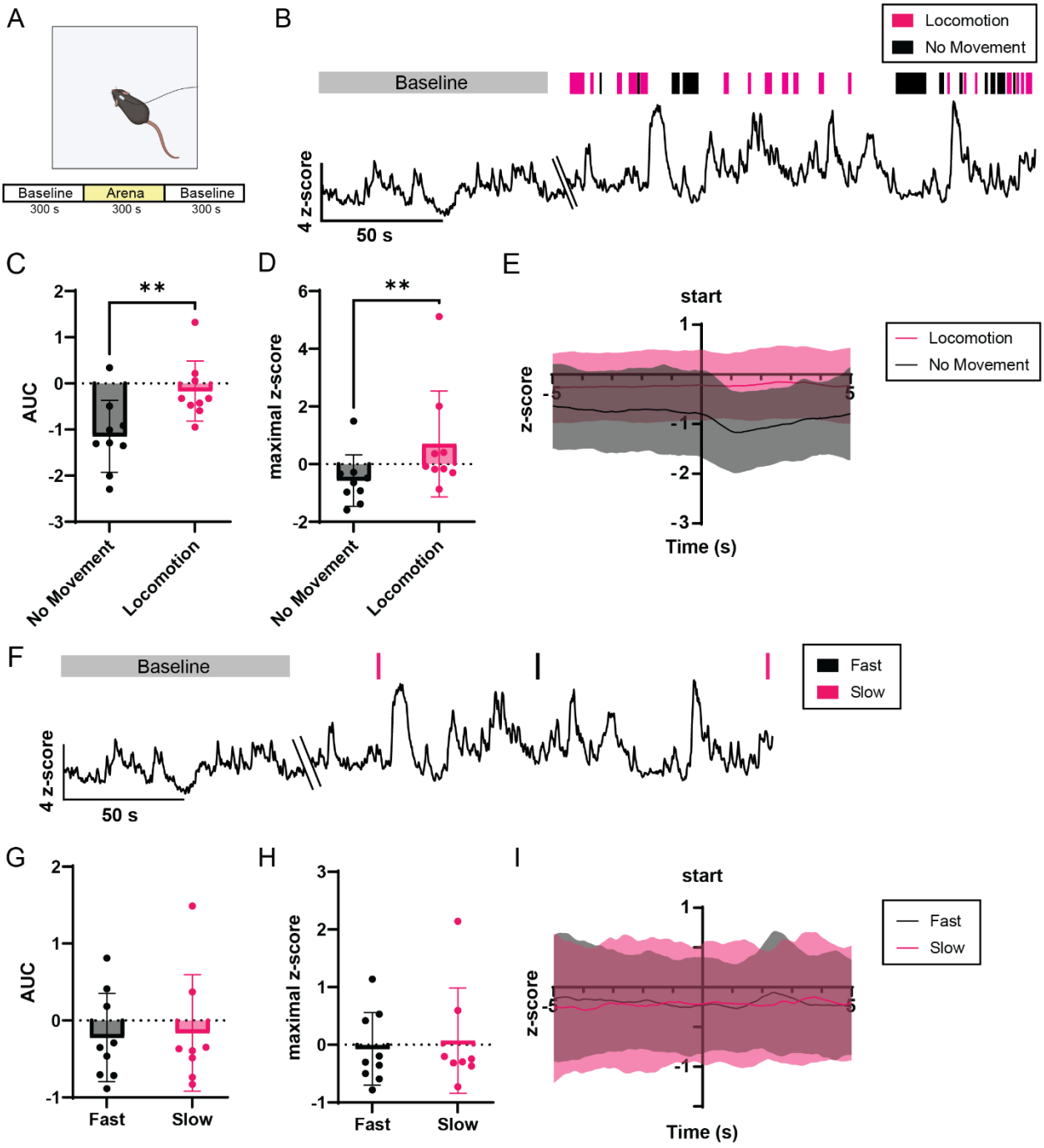

Figure 2.3. The activity of the A11 in the open field test. **A)** Diagram of the open field test. **B)** Sample trace from a representative individual showing the changes in z-score in accordance with different behaviours. The coloured bars above the trace indicate the behaviour taking place. **C)** The average area under the curve for each behaviour. Fluorescence was significantly different between locomotion and no movement behaviours (n = 9). **D)** The average maximal z-score value for each behaviour. Maximal fluorescence was significantly different between locomotion

and no movement behaviours (n = 9). **E)** Average A11 fluorescence at the onset of each behaviour centered at zero. The standard deviation for each trace is represented by the semi-transparent backgrounds. **F)** Sample trace from a representative individual showing the changes in z-score in accordance with different speeds. The coloured bars above the trace indicate the behaviour taking place. **G)** The average area under the curve for each behaviour. No significant differences were found between speeds (fast n = 9, slow n = 8). **H)** The average maximal z-score value for each speed. No significant differences were found between speeds (fast n = 9, slow n = 8). **I)** Average A11 fluorescence at the onset of each behaviour centered at zero. The standard deviation for each trace is represented by the semi-transparent backgrounds. ** = $p \leq 0.01$.

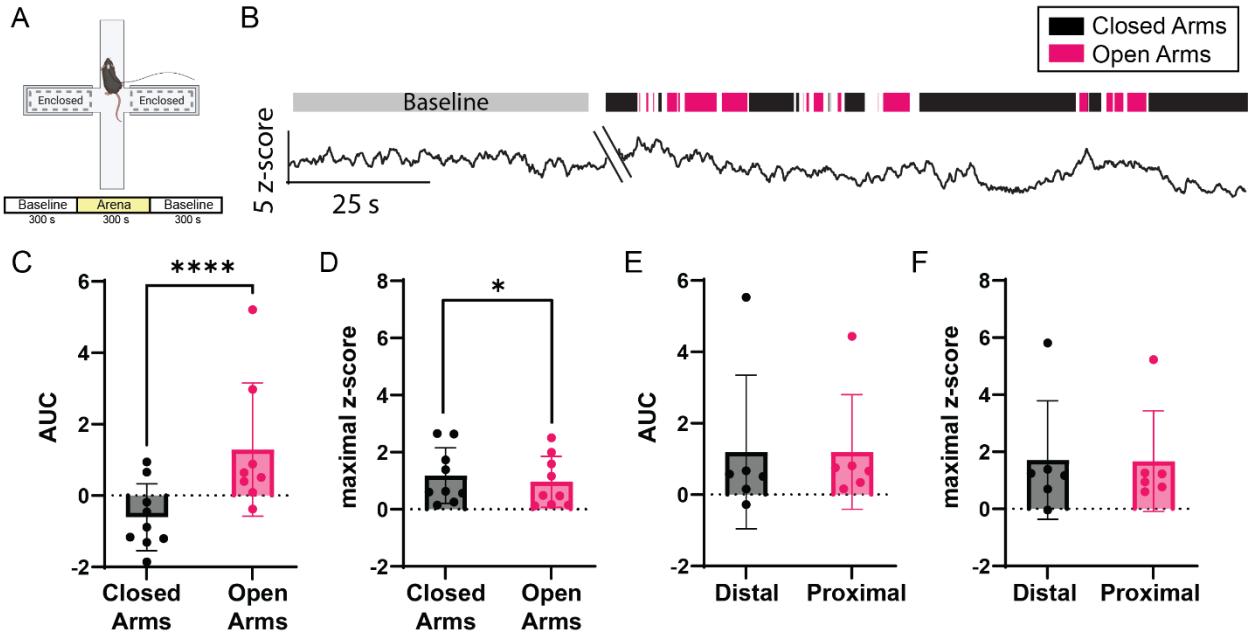

Figure 2.4. The activity of the A11 in the elevated plus maze test. **A)** Diagram of the elevated plus maze test. **B)** Sample trace from a representative individual showing the changes in z-score in accordance with different behaviours. **C)** The average area under the curve for each behaviour. A significant difference in activity was observed (n = 9). **D)** The average maximal z-score value for each behaviour. A significant difference in maximal fluorescence was found between the two regions of the EPM (n = 9). **E)** The average area under the curve for distal or proximal movements in the open arm of the EPM. No significant difference in activity was found (n = 6). **F)** Average maximal fluorescence between the two types of movement in the open arm. No significant difference was found (n = 6). **** = $p \leq 0.0001$, * = $p \leq 0.05$.

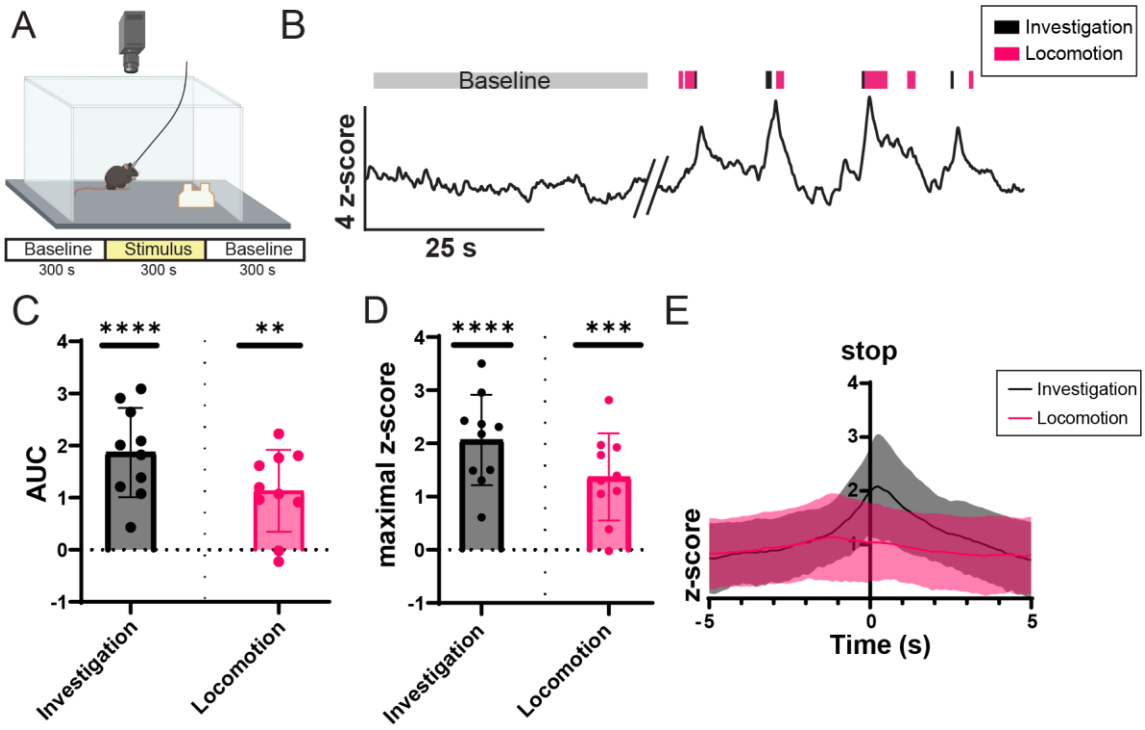

Figure 2.5. The activity of the A11 during the presentation of a novel object. **A)** Diagram of the novel object test. **B)** Sample trace of a baseline period and a period of novel object exposure. The coloured bands above the trace indicate investigation of the novel object and locomotor behaviours. **C)** Area under the curve data showing significant differences from baseline for both investigation (n = 10) and locomotion behaviours (n = 10). **D)** Maximal fluorescence data showing significant differences from baseline for both investigation (n = 10) and locomotor (n = 10) behaviours. **E)** Graph indicating the time course of the two specified behaviours. The offset of the behaviours is tethered at zero, and a peak in fluorescence is observed at the offset of the investigation behaviour, but not the locomotor behaviour. **** = $p \leq 0.0001$, *** = $p \leq 0.001$, ** = $p \leq 0.01$.

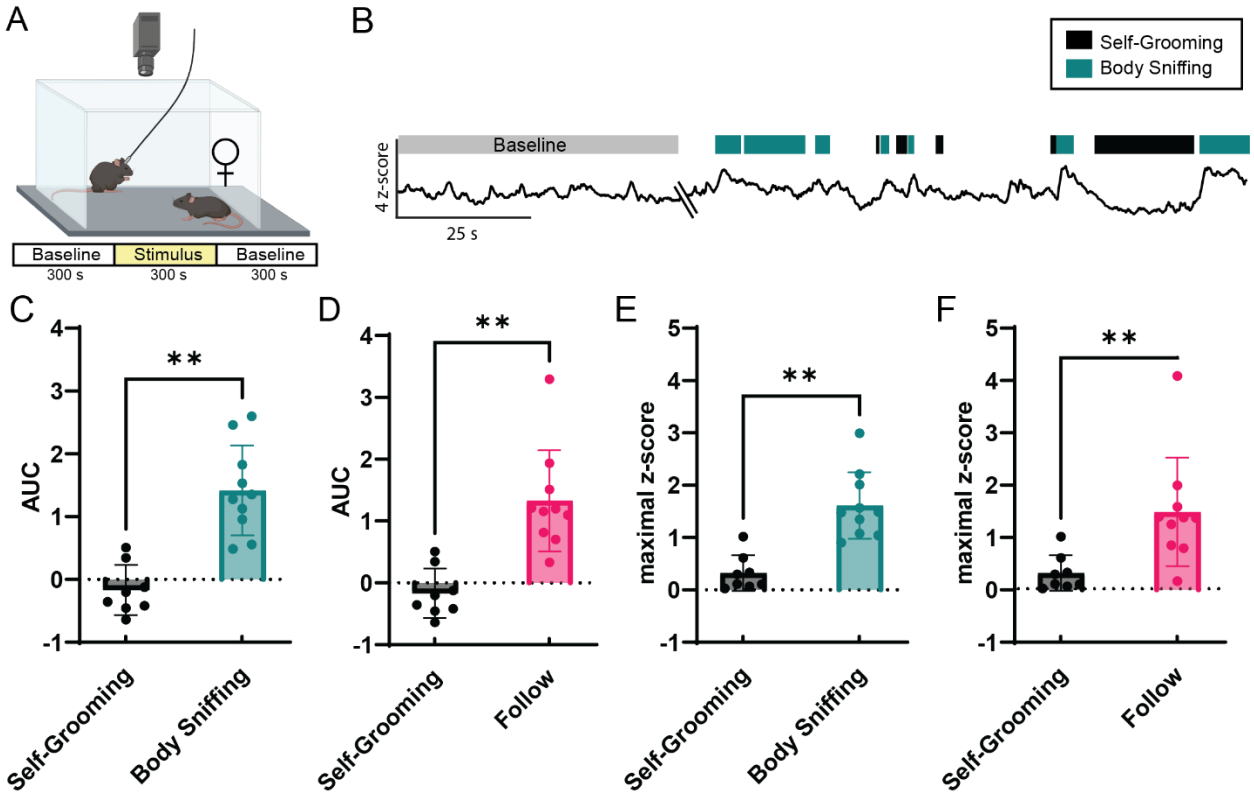

Figure 2.6. The activity of the A11 in the novel female test. **A)** Diagram of the novel female test. **B)** Sample trace from a representative individual showing the changes in z-score in accordance with different behaviours. The coloured bars above the trace indicate the behaviour taking place. **C)** Area under the curve data showing a significant difference (n = 9) between self-grooming and body sniffing. **D)** Area under the curve data showing a significant difference (n = 9) between self-grooming and follow. **E)** Maximal fluorescence data showing a significant difference between self-grooming and body sniffing (n = 9). **F)** Maximal fluorescence data showing a significant difference between self-grooming and follow (n = 9). ** = $p \leq 0.01$.

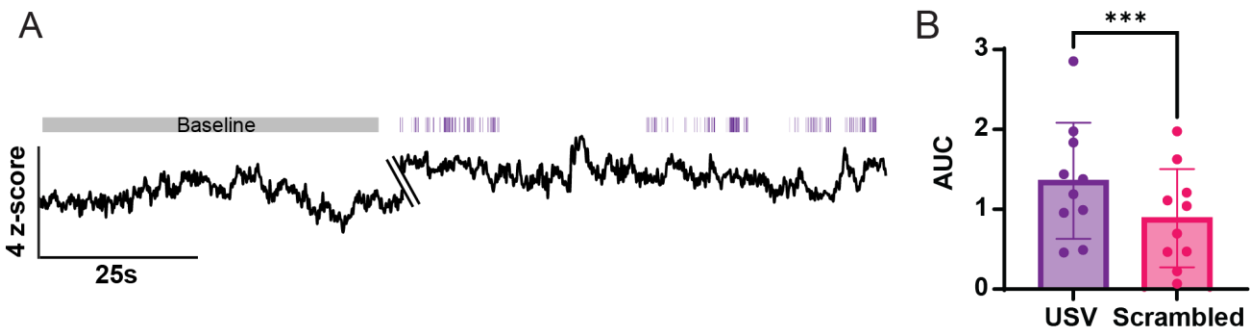

Figure 2.7. The activity of the A11 during ultrasonic vocalizations. **A)** Sample trace showing A11 activity in relation to a period without the female present (baseline) and a period with vocalizations between the male and female mice (vocalizations indicated by the purple bars above the trace). **B)** A significant difference was found in area under the curve (AUC) between USV (n = 10) and scrambled (n = 10) time points. *** = $p \leq 0.001$.

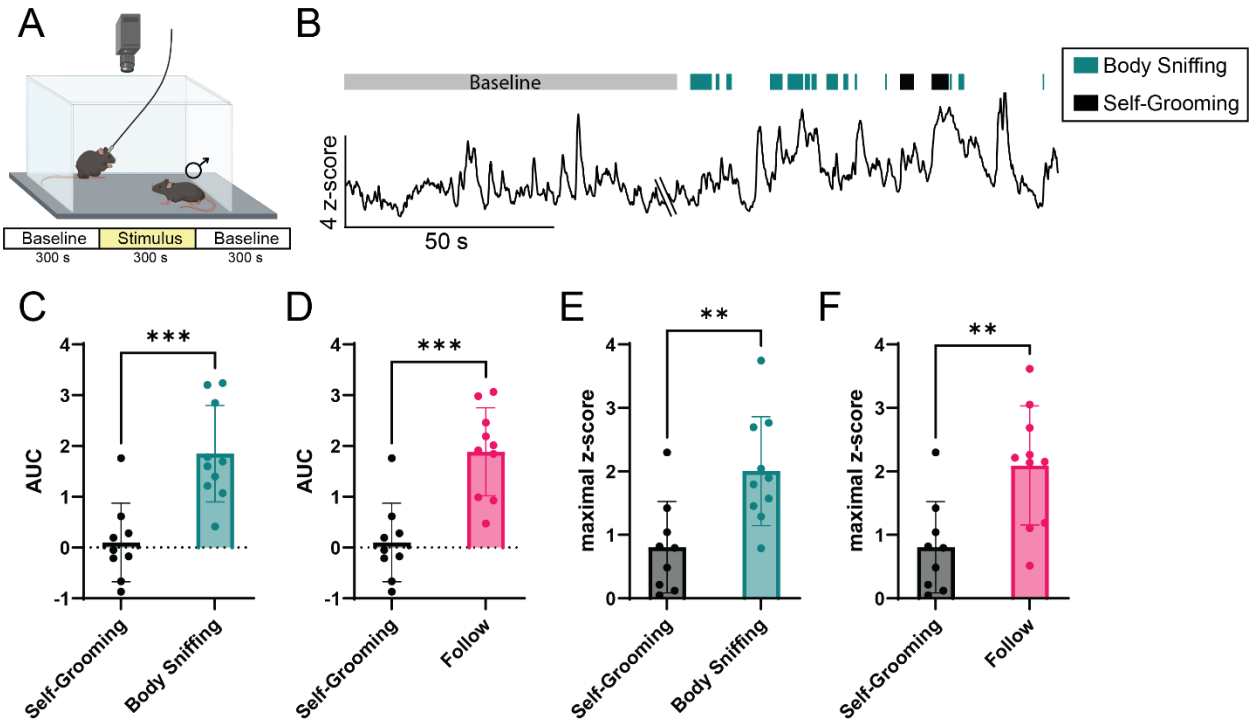

Figure 2.8. The activity of the A11 in the novel male test. **A)** Diagram of the novel male test. **B)** Sample trace showing a baseline period and a period with the intruder mouse present and certain behaviours, represented by the coloured bars above the trace. **C)** Area under the curve data demonstrating a significant difference between self-grooming and body sniffing (follow n = 10, self-grooming n = 9). **D)** Area under the curve data showing a significant difference between self-grooming and follow (follow n = 10, self-grooming n = 9). **E)** Maximal fluorescence data showing a significant difference between self-grooming and body sniffing (follow n = 10, self-grooming n = 9). **F)** Maximal fluorescence data for self-grooming and follow demonstrating a significant difference (follow n = 10, self-grooming n = 9). *** = $p \leq 0.001$, ** = $p \leq 0.01$.

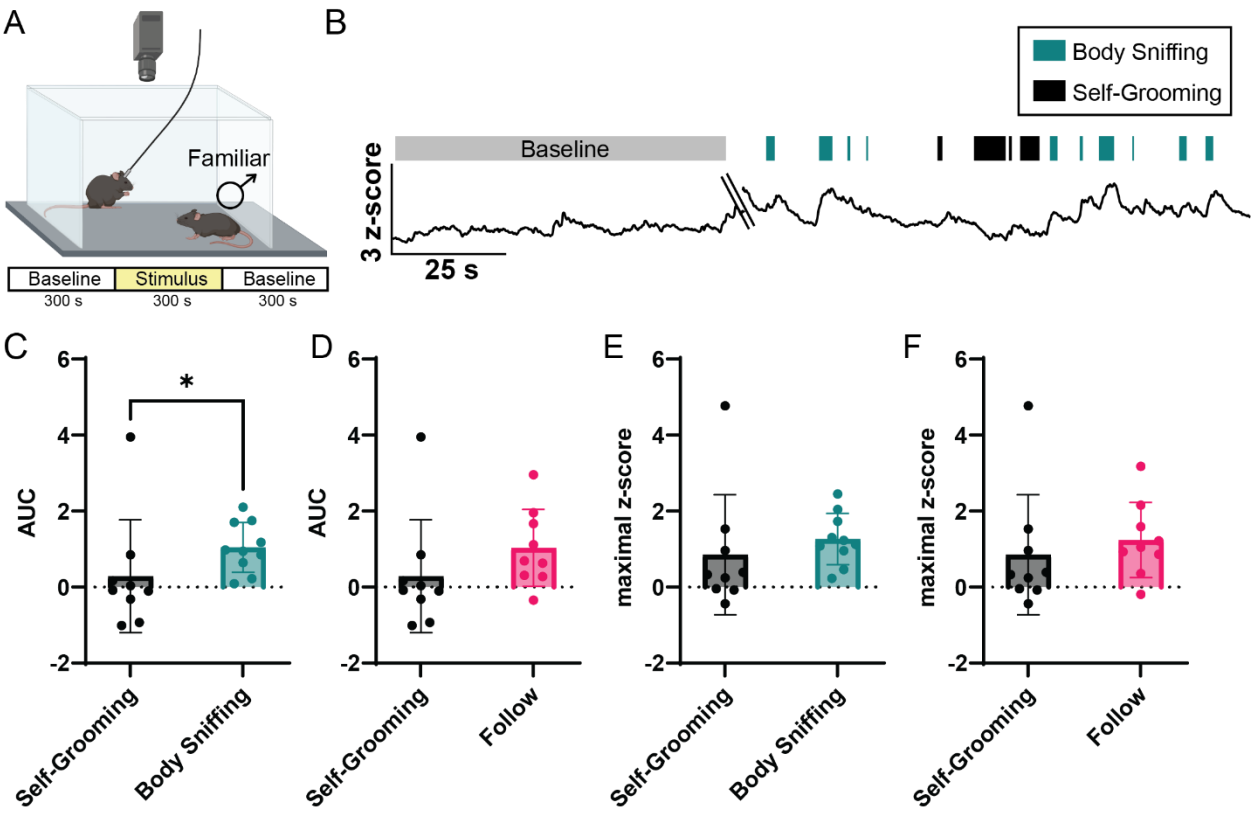

Figure 2.9. The activity of the A11 in the familiar male test. **A)** Diagram of the familiar male test. **B)** Sample trace of the A11's activity in relation to baseline or specified behaviours (the coloured bars above the trace). **C)** Area under the curve data for self-grooming and body sniffing showing a significant difference (self-grooming n = 9, body sniffing n = 10). **D)** Area under the curve data showed no significant difference between self-grooming and follow behaviours (n = 9). **E)** Maximal fluorescence data for self-grooming and body sniffing showed no significant difference (self-grooming n = 9, body sniffing n = 10). **F)** Maximal fluorescence data showing no significant difference between self-grooming and follow behaviours (n = 9). * = $p \leq 0.05$.

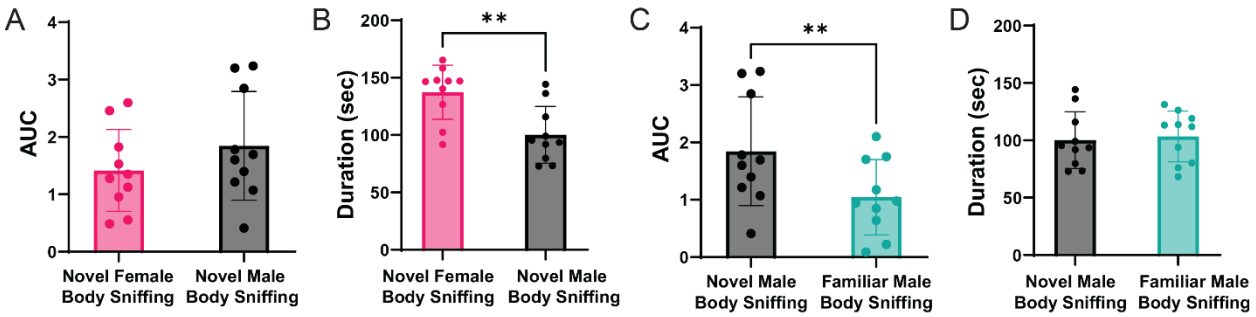

Figure 2.10. Comparisons of A11 activity during body sniffing in response to different stimuli. **A)** Area under the curve data compared between the novel female and novel male tests in relation to body sniffing behaviour. No significant difference was found. **B)** Average time spent body sniffing the novel social stimulus in either test. A significant difference was found. **C)** Area under the curve data between a novel and familiar male stimulus in the context of body sniffing. A significant difference in AUC was observed. **D)** Average time spent body sniffing the male stimulus in either test. No significant difference was found. ** = $p \leq 0.01$.

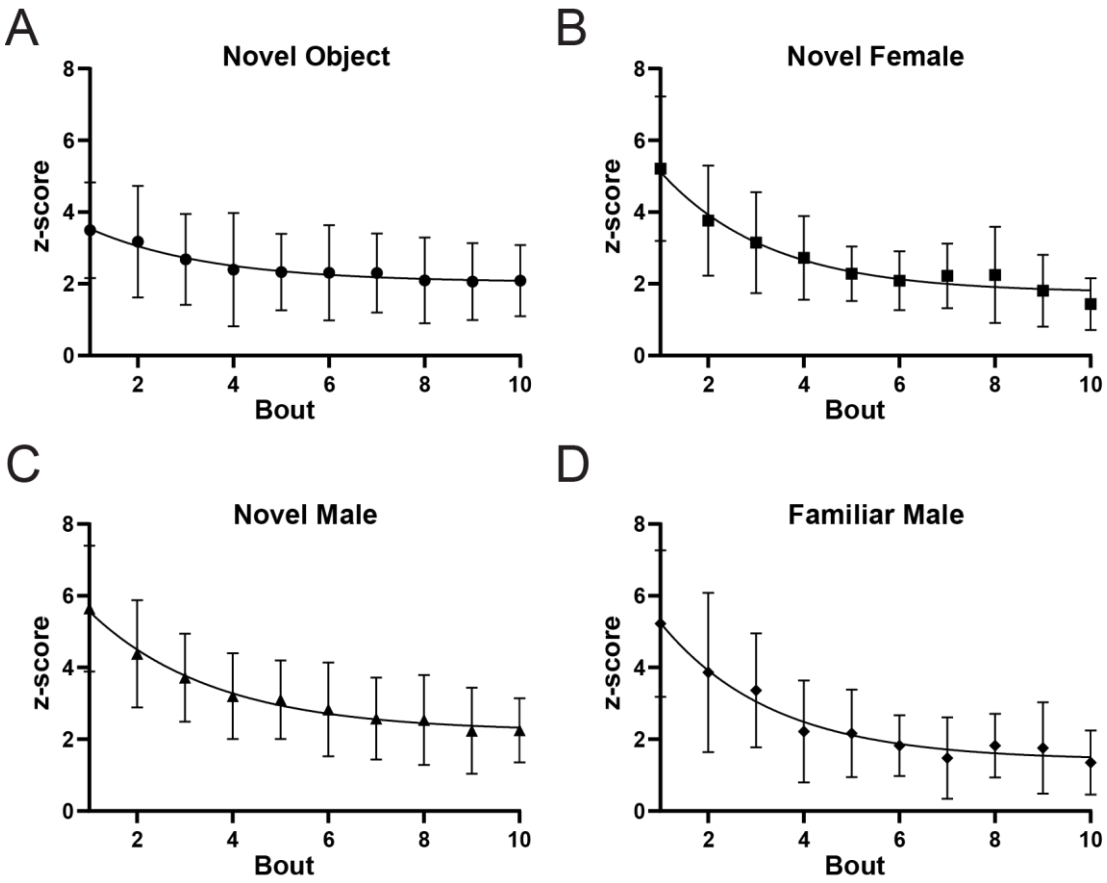

Figure 2.11. Decay in maximal fluorescence across the first 10 bouts of **A)** investigation of the novel object, **B)** body sniffing of the novel female, **C)** body sniffing of the novel male, **D)** body sniffing of the familiar male.

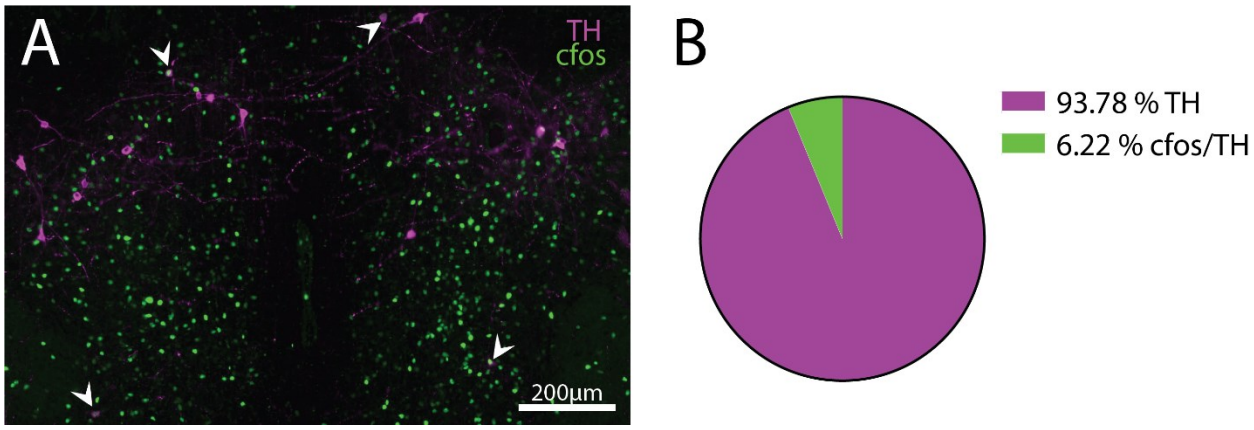

Figure 2.12. The A11 region's dopaminergic and *c-fos*-positive staining following the novel female test. **A)** Representative image of the A11 region showing dopaminergic cells (TH in magenta) and *c-fos* positive cells (green), with only a few cells demonstrating colocalization of the two signals (indicated by white arrows). **B)** Of all images across 22 mice, approximately 6% of TH^+ cells were also *c-fos*$^+$.

3. DISCUSSION & SUMMARY OF FINDINGS

3.1. Summary of Findings

This thesis has demonstrated with fibre photometry that the A11 region increases its activity in response to the presentation of novel stimuli, and in this context, locomotion is also associated with an increase in A11 activity. Also, the A11 region increases its activity during periods of ultrasonic vocalizations. Conversely, when experimental mice are locomoting in an open field, there is no significant increase in activity. Interestingly, the sex of the intruder mice did not affect A11 activity as was originally thought, considering the sexual dimorphism of the nucleus. In addition, the preliminary work presented in Appendix C demonstrated the feasibility of an intersectional approach to target spinally-projecting cells.

3.2. The A11's Activity in a Variety of Contexts

This thesis is the first to measure A11 activity in a freely moving vertebrate and presents interesting data which considers the activity of the heterogeneous cell populations of the A11, rather than cell-type specific activity. I initially hypothesized that the A11's activity would increase in response to locomotor behaviours, based upon previous research implicating the dopaminergic cells of this region in locomotion (Koblinger et al., 2018). My findings in the open field suggested that the A11's activity was significantly different between periods of no movement and periods of locomotor activity in this context, but locomotor activity did not perturb A11 fluorescence beyond baseline levels. This motivated a broader investigation of A11 activity in a wider variety of contexts. The open arms of the elevated plus maze elicited an increase in activity, suggesting that the A11 was excited by exploration of the arena during lower anxiety. When presented with various social and inanimate stimuli, the A11 responded by increasing its fluorescence during the investigation of novel stimuli. Interestingly, the activity was increased during goal-directed locomotion in these contexts, but only when the stimulus was novel. I propose that the A11, rather than encoding general locomotor behaviours, is specifically modulating its activity in response to novelty, and is potentially involved in goal-directed locomotor behaviours. Given the A11's connections to the locus coeruleus, the perirhinal cortex, the amygdala, and the hippocampus, all regions involved in responding to novelty, it is possible that these regions may begin to form a circuit through which the A11 responds to novelty (Maeda et al., 1991; Beckford, 2008; Schomaker and Meeter, 2015; Koblinger, 2017).

This thesis also investigated the role of the A11 in sociosexual functions to expand these findings to include mice. I found that A11 activity increased during ultrasonic emissions between the male-female dyad when compared to randomly selected scrambled data, which suggests that the male A11 responds to USVs; however, future work with faster calcium indicators (i.e. GCaMP7) is important to further investigate this matter (Dana et al., 2019).

The immunohistochemical results of *c-fos* activation of A11 cells following the novel female test suggest that the non-DAergic cells of this region are more active during the presentation of a novel female. This is important to consider, as very little work has explored the specific contributions of the peptidergic, glutamatergic, and GABAergic cells to behaviours, whether it be locomotor or non-locomotor.

3.3. **Future Directions**

The review of the A11 presented in Chapter 1 shows that the inputs onto the A11 are severely understudied. Previous papers have reported inputs onto the A11 based upon work targeting the posterior hypothalamic area as a whole, but the work presented in Abrahamson and Moore (2001) never specifically targeted the A11 region appropriately. One of the most important avenues of future work would be the appropriate targeting and documentation of A11 inputs, which could help inform the results of this thesis and future experiments building off these findings. With a more complete picture of A11 afferents and efferents, specific pathways could be targeted for stimulation or inactivation to elucidate the roles of specific circuits in the variety of roles served by the A11 nucleus.

In the context of the fibre photometry data presented in this thesis, further work is needed to investigate the A11's role in encoding and responding to novel stimuli (both social and inanimate). My approach recorded from the entire population of A11 cells regardless of cell type, and future work would benefit from recording activity from non-DAergic cell populations of this region (whether through fibre photometry, miniscopes, or through single-cell recordings), because those cells appeared to be more active following presentation of a novel female stimulus. It might also be interesting to record specific activity patterns from this region's GABAergic and glutamatergic cells to determine if these subpopulations play different roles or respond differently to novelty. In addition, more specific information regarding cell-type-specific

activity could be quickly gained by immunohistochemical methods which would search for overlap between *c-fos* and glutamatergic, peptidergic, or GABAergic markers.

Further work could stimulate or inhibit specific cell populations of this region during the exploration of novel stimuli to determine if this region is mediating novelty responses or simply encoding the novel stimuli by replicating the current experiments in addition to a familiar female test and a standard object recognition task.

In addition, the current data suggest that the A11 encodes ultrasonic vocalizations, which would be worthwhile to explore in female mice, as female dyads have been shown to emit vocalizations (Premoli et al., 2021). The inclusion of female mice in future studies is of great importance. The A11's sexual dimorphism and roles in sociosexual behaviours in mice and other vertebrates show the necessity of research involving both sexes. It is possible that the female A11 responds differently to novel stimuli or sociosexual behaviours than was presented in this thesis.

In the context of the optogenetic work presented in appendix C, the intersectional viral approach was validated to target spinally-projecting A11 cells. A major limitation of this work, and the reason it was not further pursued by increasing sample sizes, was a methodological limitation of the approach: the intersectional viral approach that was employed only labelled and transfected a subset of A11 cells, which was by design, but the location of the fibre-optic cannula implantation further limited the number of transfected cells which were in the path of the cone of light emitted from the fibre-optic cannula. As a result, even if the entire population of A11-spinal cord cells were labelled with channelrhodopsin, given they were spread through the rostrocaudal extent of the nucleus, only a subpopulation of these cells was properly illuminated. The choice of the optogenetic approach was perhaps not the ideal method for targeting this circuit. Future work should explore the use of DREADDs in combination with this dual viral injection. Though the injection of a virus into the spinal cord may cause damage, it is unlikely as there were no locomotor deficits observed following the surgery. In addition to using DREADDs, another approach that would address the potential damage to the spinal cord would be to target the A11 with a Cre-inducible DREADD virus into a TH-Cre mouse line and the subsequent intrathecal administration of clozapine-N-oxide to preferentially stimulate the A11-spinal cord circuit.

In terms of the implications of this work in health, the A11's well-defined role in nociception means that there is more work to be done. Dysfunction of the A11 may underlie migraine, and pain perception may be an exciting avenue to integrate this thesis' findings with the current knowledge. Overall, the A11 remains understudied, and its relative contributions to functions other than nociception are also worth exploring in the future.

REFERENCES

Abdallah K, Monconduit L, Artola A, Luccarini P, Dallel R (2015) GABAAergic inhibition or dopamine denervation of the A11 hypothalamic nucleus induces trigeminal analgesia. Pain 156:644–655.

Abrahamson EE, Moore RY (2001) The posterior hypothalamic area: chemoarchitecture and afferent connections. Brain Res 889:1–22.

Ahmadlou M, Houba JHW, van Vierbergen JFM, Giannouli M, Gimenez G-A, van Weeghel C, Darbanfouladi M, Shirazi MY, Dziubek J, Kacem M, de Winter F, Heimel JA (2021) A cell type-specific cortico-subcortical brain circuit for investigatory and novelty-seeking behavior. Science 372:1–9.

Aragona BJ, Liu Y, Curtis JT, Stephan FK, Wang Z (2003) A critical role for nucleus accumbens dopamine in partner-preference formation in male prairie voles. J Neurosci 23:3483–3490.

Arrant AE, Schramm-Sapyta NL, Kuhn CM (2013) Use of the light/dark test for anxiety in adult and adolescent male rats. Behav Brain Res 256:119–127.

Avery MC, Krichmar JL (2017) Neuromodulatory Systems and Their Interactions: A Review of Models, Theories, and Experiments. Front Neural Circuits 11:1–18.

Bäck S, Dossat A, Parkkinen I, Koivula P, Airavaara M, Richie CT, Chen Y-H, Wang Y, Harvey BK (2019) Neuronal Activation Stimulates Cytomegalovirus Promoter-Driven Transgene Expression. Mol Ther Methods Clin Dev 14:180–188.

Banerjee SB, Dias BG, Crews D, Adkins-Regan E (2013) Newly paired zebra finches have higher dopamine levels and immediate early gene Fos expression in dopaminergic neurons. Eur J Neurosci 38:3731–3739.

Barraud Q, Obeid I, Aubert I, Barrière G, Contamin H, McGuire S, Ravenscroft P, Porras G, Tison F, Bezard E, Ghorayeb I (2010) Neuroanatomical study of the A11 diencephalospinal pathway in the non-human primate. PLoS One 5:1–14.

Beckford GEH (2008) The functional organization and behavioral relevance of the A11 hypothalamospinal dopaminergic system. Available at: http://search.proquest.com/openview/afc3a1a04eccd1d36ffc088352fdfe9e/1?pq-origsite=gscholar&cbl=18750&diss=y&casa_token=sOHjbDtsEiAAAAAA:haeECjaQkWA7_xolM-tArrVYZfqAqRdmxkkT7d5wR0VMSt7eBxVdlIv32DnDs9v8mfGN41H7.

Beninger RJ (1983) The role of dopamine in locomotor activity and learning. Brain Res 287:173–196.

Berns KI, Giraud C (1996) Biology of Adeno-associated Virus. In: Adeno-Associated Virus (AAV) Vectors in Gene Therapy (Berns KI, Giraud C, eds), pp 1–23 Current Topics in Microbiology and Immunology. Berlin, Heidelberg: Springer.

Bharati IS, Goodson JL (2006) Fos responses of dopamine neurons to sociosexual stimuli in male zebra finches. Neuroscience 143:661–670.

Billings BK, Bhagwandin A, Patzke N, Ngwenya A, Rook N, von Eugen K, Tabrik S, Güntürkün O, Manger PR (2020) Nuclear organization and morphology of catecholaminergic neurons and certain pallial terminal networks in the brain of the Nile crocodile, Crocodylus niloticus. J Chem Neuroanat 109:101851.

Bimpisidis Z, König N, Wallén-Mackenzie Å (2020) Two Different Real-Time Place Preference Paradigms Using Optogenetics within the Ventral Tegmental Area of the Mouse. J Vis Exp 156:1–11.

Björklund A, Lindvall O (1984) Dopamine-containing systems in the CNS. In: Handbook of Chemical Neuroanatomy Vol. 2: Classical Transmitters in the CNS, Part I (Björklund A, Hökfelt T, eds), pp 55–122. Elsevier Science Publishers.

Blessing WW, Chalmers JP (1979) Direct projection of catecholamine (possibly dopamine)-containing neurons from hypothalamus to spinal cord. Neurosci Lett 11:35–40.

Bouvier J, Caggiano V, Leiras R, Caldeira V, Bellardita C, Balueva K, Fuchs A, Kiehn O (2015) Descending Command Neurons in the Brainstem that Halt Locomotion. Cell 163:1191–1203.

Calabresi P, Picconi B, Tozzi A, Ghiglieri V, Di Filippo M (2014) Direct and indirect pathways of basal ganglia: a critical reappraisal. Nat Neurosci 17:1022–1030.

Cassidy RM, Lu Y, Jere M, Tian J-B, Xu Y, Mangieri LR, Felix-Okoroji B, Selever J, Xu Y, Arenkiel BR, Tong Q (2019) A lateral hypothalamus to basal forebrain neurocircuit promotes feeding by suppressing responses to anxiogenic environmental cues. Sci Adv 5:1–11.

Cearley CN, Wolfe JH (2006) Transduction characteristics of adeno-associated virus vectors expressing cap serotypes 7, 8, 9, and Rh10 in the mouse brain. Mol Ther 13:528–537.

Cechetto DF, Saper CB (1988) Neurochemical organization of the hypothalamic projection to the spinal cord in the rat. J Comp Neurol 272:579–604.

Chang SJ, Santamaria AJ, Sanchez FJ, Villamil LM, Saraiva PP, Benavides F, Nunez-Gomez Y, Solano JP, Opris I, Guest JD, Noga BR (2021) Deep brain stimulation of midbrain locomotor circuits in the freely moving pig. Brain Stimul 14:467–476.

Charbit AR, Akerman S, Goadsby PJ (2011) Trigeminocervical complex responses after lesioning dopaminergic A11 nucleus are modified by dopamine and serotonin mechanisms. Pain 152:2365–2376.

Charbit AR, Akerman S, Holland PR (2009) Neurons of the Dopaminergic/Calcitonin Gene-Related Peptide A11 Cell Group Modulate Neuronal Firing in the Trigeminocervical Complex: An Electrophysiological and Immunohistochemical Study. J Neurosci 29:12532–12541.

Charlier TD, Ball GF, Balthazart J (2005) Sexual behavior activates the expression of the immediate early genes c-fos and Zenk (egr-1) in catecholaminergic neurons of male Japanese quail. Neuroscience 131:13–30.

Chen J, Markowitz JE, Lilascharoen V, Taylor S, Sheurpukdi P, Keller JA, Jensen JR, Lim BK, Datta SR, Stowers L (2021) Flexible scaling and persistence of social vocal communication. Nature 593:108–113.

Chen T-W, Wardill TJ, Sun Y, Pulver SR, Renninger SL, Baohan A, Schreiter ER, Kerr RA, Orger MB, Jayaraman V, Looger LL, Svoboda K, Kim DS (2013) Ultrasensitive fluorescent proteins for imaging neuronal activity. Nature 499:295–300.

Cho JR, Treweek JB, Robinson JE, Xiao C, Bremner LR, Greenbaum A, Gradinaru V (2017) Dorsal Raphe Dopamine Neurons Modulate Arousal and Promote Wakefulness by Salient Stimuli. Neuron 94:1205–1219.

Choi S (2018) Systemic investigation of D-cells in the mouse central nervous system. Undergraduate thesis, University of Calgary, Calgary.

Christie KJ, Whelan PJ (2005) Monoaminergic establishment of rostrocaudal gradients of rhythmicity in the neonatal mouse spinal cord. J Neurophysiol 94:1554–1564.

Clemens S, Rye D, Hochman S (2006) Restless legs syndrome: Revisiting the dopamine hypothesis from the spinal cord perspective. Neurology 67:125–130.

Cregg JM, Leiras R, Montalant A, Wanken P, Wickersham IR, Kiehn O (2020) Brainstem neurons that command mammalian locomotor asymmetries. Nat Neurosci 23:730–740.

Dahlström A, Fuxe K (1964) Evidence for the existence of monoamine-containing neurons in the central nervous system. Acta Physiologica Scandinavia 62 Available at: https://www.ncbi.nlm.nih.gov/pubmed/14229500.

Damdindorj L, Karnan S, Ota A, Hossain E, Konishi Y, Hosokawa Y, Konishi H (2014) A comparative analysis of constitutive promoters located in adeno-associated viral vectors. PLoS One 9:1–10.

Dana H, Sun Y, Mohar B, Hulse BK, Kerlin AM, Hasseman JP, Tsegaye G, Tsang A, Wong A, Patel R, Macklin JJ, Chen Y, Konnerth A, Jayaraman V, Looger LL, Schreiter ER, Svoboda K, Kim DS (2019) High-performance calcium sensors for imaging activity in neuronal populations and microcompartments. Nat Methods 16:649–657.

Daviu N, Füzesi T, Rosenegger DG, Rasiah NP, Sterley T-L, Peringod G, Bains JS (2020) Paraventricular nucleus CRH neurons encode stress controllability and regulate defensive behavior selection. Nat Neurosci 23:398–410.

Dayton RD, Wang DB, Klein RL (2012) The advent of AAV9 expands applications for brain and spinal cord gene delivery. Expert Opin Biol Ther 12:757–766.

Dugué GP, Akemann W, Knöpfel T (2012) Chapter 1 - A comprehensive concept of optogenetics. In: Progress in Brain Research (Knöpfel T, Boyden ES, eds), pp 1–28. Elsevier.

Duysens J, Van de Crommert HWAA (1998) Neural control of locomotion; Part 1: The central pattern generator from cats to humans. Gait Posture 7:131–141.

Earley CJ, Allen RP, Connor JR, Ferrucci L, Troncoso J (2009) The dopaminergic neurons of the A11 system in RLS autopsy brains appear normal. Sleep Med 10:1155–1157.

Esteves AM, Lopes C, Frank MK, Arida RM, Frussa-Filho R, Tufik S, de Mello MT (2016) Can physical exercise have a protective effect in an animal model of sleep-related movement disorder? Brain Res 1639:47–57.

Fink JS, Smith GP (1980) Mesolimbicocortical dopamine terminal fields are necessary for normal locomotor and investigatory exploration in rats. Brain Res 199:359–384.

Fleetwood-Walker SM, Hope PJ, Mitchell R (1988) Antinociceptive actions of descending dopaminergic tracts on cat and rat dorsal horn somatosensory neurones. J Physiol 399:335–348.

Fonseca AH, Santana GM, Bosque Ortiz GM, Bampi S, Dietrich MO (2021) Analysis of ultrasonic vocalizations from mice using computer vision and machine learning. Elife 10:1–22.

Fougère M, van der Zouwen CI, Boutin J, Ryczko D (2021) Heterogeneous expression of dopaminergic markers and Vglut2 in mouse mesodiencephalic dopaminergic nuclei A8-A13. J Comp Neurol 529:1273–1292.

Franklin KBJ, Paxinos G (2008) The Mouse Brain In Sterotaxic Coordinates (Third Edition). Academic Press.

Friard O, Gamba M (2016) BORIS : a free, versatile open-source event-logging software for video/audio coding and live observations. Methods Ecol Evol 7:1325–1330.

Friston KJ, Shiner T, FitzGerald T, Galea JM, Adams R, Brown H, Dolan RJ, Moran R, Stephan KE, Bestmann S (2012) Dopamine, affordance and active inference. PLoS Comput Biol 8:1–20.

Gao X-M, Elmer GI, Adams-Huet B, Tamminga CA (2009) Social memory in mice: disruption with an NMDA antagonist and attenuation with antipsychotic drugs. Pharmacol Biochem Behav 92:236–242.

Gerin C, Privat A (1998) Direct evidence for the link between monoaminergic descending pathways and motor activity: II. A study with microdialysis probes implanted in the ventral horn of the spinal cord. Brain Res 794:169–173.

Gordon IT, Whelan PJ (2006) Deciphering the organization and modulation of spinal locomotor central pattern generators. J Exp Biol 209:2007–2014.

Gore BB, Soden ME, Zweifel LS (2013) Manipulating gene expression in projection-specific neuronal populations using combinatorial viral approaches. Curr Protoc Neurosci 65:4.35.1-20.

Gossard TR, Trotti LM, Videnovic A, St Louis EK (2021) Restless Legs Syndrome: Contemporary Diagnosis and Treatment. Neurotherapeutics 18:140–155.

Gould TD, Dao DT, Kovacsics CE (2009) The Open Field Test. In: Mood and Anxiety Related Phenotypes in Mice: Characterization Using Behavioral Tests (Gould TD, ed), pp 1–20. Totowa, NJ: Humana Press.

Goulding M (2009) Circuits controlling vertebrate locomotion: moving in a new direction. Nat Rev Neurosci 10:507–518.

Grams JR, Nelson TL, Tran MA, Elliott DA, Whelan PJ (2021) Uncovering the descending dopaminergic inputs to the medullary reticular formation [abstract]. In: Neuroscience 2022 , November 8-11 2022, Chicago, IL.

Gray SJ, Samulski RJ (2011) Vector Design and Considerations for CNS Applications. In: Gene Vector Design and Application to Treat Nervous System Disorders (Glorioso J, ed), pp 9–15. Washington, DC: Society for Neuroscience.

Gunaydin LA, Grosenick L, Finkelstein JC, Kauvar IV, Fenno LE, Adhikari A, Lammel S, Mirzabekov JJ, Airan RD, Zalocusky KA, Tye KM, Anikeeva P, Malenka RC, Deisseroth K (2014) Natural neural projection dynamics underlying social behavior. Cell 157:1535–1551.

Haggerty DL, Grecco GG, Reeves KC, Atwood B (2020) Adeno-Associated Viral Vectors in Neuroscience Research. Mol Ther Methods Clin Dev 17:69–82.

Hammerschmidt K, Radyushkin K, Ehrenreich H, Fischer J (2012) The structure and usage of female and male mouse ultrasonic vocalizations reveal only minor differences. PLoS One 7:e41133.

Han P, Nakanishi ST, Tran MA, Whelan PJ (2007) Dopaminergic modulation of spinal neuronal excitability. J Neurosci 27:13192–13204.

Harris-Warrick RM, Cohen AH (1985) Serotonin modulates the central pattern generator for locomotion in the isolated lamprey spinal cord. J Exp Biol 116:27–46.

Hasue RH, Shammah-Lagnado SJ (2002) Origin of the dopaminergic innervation of the central extended amygdala and accumbens shell: a combined retrograde tracing and immunohistochemical study in the rat. J Comp Neurol 454:15–33.

Hökfelt T, Johansson O, Fuxe K, Goldstein M, Park D (1976) Immunohistochemical studies on the localization and distribution of monoamine neuron systems in the rat brain I. Tyrosine hydroxlase in the mes- and diencephalon. Medical Biology 54:427–453.

Hökfelt T, Mårtensson R, Björklund A, Kleinau S, Goldstein M (1984) Distributional maps of tyrosine-hydroxylase-immunoreactive neurons in the rat brain. In: Handbook of Chemical Neuroanatomy Vol. 2: Classical Transmitters in the CNS, Part I (Björklund A, Hökfelt T, eds), pp 277–379. Amsterdam: Elsevier Science Publishers B.V.

Holstege G, Georgiadis JR, Paans AMJ, Meiners LC, van der Graaf FHCE, Reinders AATS (2003) Brain activation during human male ejaculation. J Neurosci 23:9185–9193.

Holstege JC, Van Dijken H, Buijs RM, Goedknegt H, Gosens T, Bongers CM (1996) Distribution of dopamine immunoreactivity in the rat, cat and monkey spinal cord. J Comp Neurol 376:631–652.

Huang ZJ, Zeng H (2013) Genetic approaches to neural circuits in the mouse. Annu Rev Neurosci 36:183–215.

Iwasaki M, Poulsen TM, Oka K, Hessler NA (2014) Sexually dimorphic activation of dopaminergic areas depends on affiliation during courtship and pair formation. Front Behav Neurosci 8:1–10.

Jaeger CB, Teitelman G, Joh TH, Albert VR, Park DH, Reis DJ (1983) Some neurons of the rat central nervous system contain aromatic-L-amino-acid decarboxylase but not monoamines. Science 219:1233–1235.

Jensen TS, Smith DF (1982) Dopaminergic effects on tail-flick response in spinal rats. Eur J Pharmacol 79:129–133.

Jensen TS, Yaksh TL (1984) Effects of an intrathecal dopamine agonist, apomorphine, on thermal and chemical evoked noxious responses in rats. Brain Res 296:285–293.

Jerzemowska G, Plucińska K, Kuśmierczak M, Myślińska D, Orzeł-Gryglewska J (2014) Locomotor response to novelty correlates with differences in number and morphology of hypothalamic tyrosine hydroxylase positive cells in rats. Brain Res Bull 101:26–36.

Kagan R, Kainz V, Burstein R, Noseda R (2013) Hypothalamic and basal ganglia projections to the posterior thalamus: possible role in modulation of migraine headache and photophobia. Neuroscience 248:359–368.

Kandel ER, Mack S, Jessell TM, Schwartz JH, Siegelbaum SA, Hudspeth AJ (2013) Principles of Neural Science, Fifth Edition. McGraw Hill Professional.

Kawano M, Kawasaki A, Sakata-Haga H, Fukui Y, Kawano H, Nogami H, Hisano S (2006) Particular subpopulations of midbrain and hypothalamic dopamine neurons express vesicular glutamate transporter 2 in the rat brain. J Comp Neurol 498:581–592.

Kiehn O, Dougherty K (2013) Locomotion: Circuits and Physiology. In: Neuroscience in the 21st Century: From Basic to Clinical (Pfaff DW, ed), pp 1209–1236. New York, NY: Springer New York.

Kim LH, Sharma S, Sharples SA, Mayr KA, Kwok CHT, Whelan PJ (2017) Integration of Descending Command Systems for the Generation of Context-Specific Locomotor Behaviors. Front Neurosci 11:1–19.

Koblinger K (2017) Characterization and Behavioural Relevance of the A11 Hypothalamospinal Dopaminergic System in the Mouse. PhD thesis, University of Calgary, Calgary. Available at: https://prism.ucalgary.ca/handle/11023/3679.

Koblinger K, Füzesi T, Ejdrygiewicz J, Krajacic A, Bains JS, Whelan PJ (2014) Characterization of A11 neurons projecting to the spinal cord of mice. PLoS One 9:1–12.

Koblinger K, Jean-Xavier C, Sharma S, Füzesi T, Young L, Eaton SEA, Kwok CHT, Bains JS, Whelan PJ (2018) Optogenetic Activation of A11 Region Increases Motor Activity. Front Neural Circuits 12:86.

Kosse C, Burdakov D (2019) Natural hypothalamic circuit dynamics underlying object memorization. Nat Commun 10:1–8.

Kügler S, Meyn L, Holzmüller H, Gerhardt E, Isenmann S, Schulz JB, Bähr M (2001) Neuron-specific expression of therapeutic proteins: evaluation of different cellular promoters in recombinant adenoviral vectors. Mol Cell Neurosci 17:78–96.

Lambert AM, Bonkowsky JL, Masino MA (2012) The conserved dopaminergic diencephalospinal tract mediates vertebrate locomotor development in zebrafish larvae. J Neurosci 32:13488–13500.

Lanciego JL, Luquin N, Obeso JA (2012) Functional neuroanatomy of the basal ganglia. Cold Spring Harb Perspect Med 2:1–21.

Le VA, Sterley T-L, Cheng N, Bains JS, Murari K (2021) Markerless mouse tracking for social experiments. bioRxiv:2021.10.20.464614 Available at: https://www.biorxiv.org/content/10.1101/2021.10.20.464614v2 [Accessed December 6, 2021].

Li L, Tang Y, Sun L, Rahman K, Huang K, Xu W, Yu J, Dai J, Cao G (2017) In vivo fiber photometry of neural activity in response to optogenetically manipulated inputs in freely moving mice. J Innov Opt Health Sci 10:1743001-1–12.

Li Y, Liu Z, Guo Q, Luo M (2019) Long-term Fiber Photometry for Neuroscience Studies. Neurosci Bull 35:425–433.

Lindvall O, Björklund A, Skagerberg G (1983) Dopamine-containing neurons in the spinal cord: anatomy and some functional aspects. Ann Neurol 14:255–260.

Liu S, Tang Y, Shu H, Tatum D, Bai Q, Crawford J, Xing Y, Lobo MK, Bellinger L, Kramer P, Tao F (2019) Dopamine receptor D2, but not D1, mediates descending dopaminergic pathway–produced analgesic effect in a trigeminal neuropathic pain mouse model. Pain 160:334–344.

Lorbach M, Kyriakou EI, Poppe R, van Dam EA, Noldus LPJJ, Veltkamp RC (2018) Learning to recognize rat social behavior: Novel dataset and cross-dataset application. J Neurosci Methods 300:166–172.

Madriaga MA, McPhee LC, Chersa T, Christie KJ, Whelan PJ (2004) Modulation of locomotor activity by multiple 5-HT and dopaminergic receptor subtypes in the neonatal mouse spinal cord. J Neurophysiol 92:1566–1576.

Maeda T, Kojima Y, Arai R, Fujimiya M, Kimura H, Kitahama K, Geffard M (1991) Monoaminergic interaction in the central nervous system: a morphological analysis in the locus coeruleus of the rat. Comp Biochem Physiol C 98:193–202.

Maler L, Ellis WG (1987) Inter-male aggressive signals in weakly electric fish are modulated by monoamines. Behav Brain Res 25:75–81.

Markakis EA, Vives KP, Bober J, Leichtle S, Leranth C, Beecham J, Elsworth JD, Roth RH, Samulski RJ, Redmond DE (2010) Comparative Transduction Efficiency of AAV Vector Serotypes 1–6 in the Substantia Nigra and Striatum of the Primate Brain. Mol Ther 18:588–593.

Martianova E, Aronson S, Proulx CD (2019) Multi-Fiber Photometry to Record Neural Activity in Freely-Moving Animals. J Vis Exp 152:e60278.

Matthews GA, Nieh EH, Vander Weele CM, Halbert SA, Pradhan RV, Yosafat AS, Glober GF, Izadmehr EM, Thomas RE, Lacy GD, Wildes CP, Ungless MA, Tye KM (2016) Dorsal Raphe Dopamine Neurons Represent the Experience of Social Isolation. Cell 164:617–631.

McLellan MA, Rosenthal NA, Pinto AR (2017) Cre-loxP-Mediated Recombination: General Principles and Experimental Considerations. Curr Protoc Mouse Biol 7:1–12.

Megat S, Shiers S, Moy JK, Barragan-Iglesias P, Pradhan G, Seal RP, Dussor G, Price TJ (2018) A Critical Role for Dopamine D5 Receptors in Pain Chronicity in Male Mice. J Neurosci 38:379–397.

Meiser J, Weindl D, Hiller K (2013) Complexity of dopamine metabolism. Cell Commun Signal 11:1–18.

Menegas W, Akiti K, Amo R, Uchida N, Watabe-Uchida M (2018) Dopamine neurons projecting to the posterior striatum reinforce avoidance of threatening stimuli. Nat Neurosci 21:1421–1430.

Messanvi F, Eggens-Meijer E, Roozendaal B, van der Want JJ (2013) A discrete dopaminergic projection from the incertohypothalamic A13 cell group to the dorsolateral periaqueductal gray in rat. Front Neuroanat 7:1–14.

Moore RY, Bloom FE (1978) Neuron systems: Anatomy and physiology of the dopamine systems. Annu Rev Neurosci 1:129–169.

Mouchet P, Guerin B, Feuerstein C (1982) Dissociate destruction of noradrenaline and dopamine descending projections in the thoracic spinal cord of the rat. Life Sci 30:373–381.

Nadim F, Bucher D (2014) Neuromodulation of neurons and synapses. Curr Opin Neurobiol 29:48–56.

Nakai J, Ohkura M, Imoto K (2001) A high signal-to-noise Ca(2+) probe composed of a single green fluorescent protein. Nat Biotechnol 19:137–141.

Nakamori H, Naitou K, Horii Y, Shimaoka H, Horii K, Sakai H, Yamada A, Furue H, Shiina T, Shimizu Y (2019) Roles of the noradrenergic nucleus locus coeruleus and dopaminergic nucleus A11 region as supraspinal defecation centers in rats. Am J Physiol Gastrointest Liver Physiol 317:G545–G555.

Nestler EJ (1994) Hard target: understanding dopaminergic neurotransmission. Cell 79:923–926.

Nevue AA, Felix RA 2nd, Portfors CV (2016) Dopaminergic projections of the subparafascicular thalamic nucleus to the auditory brainstem. Hear Res 341:202–209.

Nieh EH, Vander Weele CM, Matthews GA, Presbrey KN, Wichmann R, Leppla CA, Izadmehr EM, Tye KM (2016) Inhibitory Input from the Lateral Hypothalamus to the Ventral Tegmental Area Disinhibits Dopamine Neurons and Promotes Behavioral Activation. Neuron 90:1286–1298.

Nieuwenhuis B, Haenzi B, Hilton S, Carnicer-Lombarte A, Hobo B, Verhaagen J, Fawcett JW (2020) Optimization of adeno-associated viral vector-mediated transduction of the corticospinal tract: comparison of four promoters. Gene Ther 28:56–74.

Noga BR, Kettler J, Jordan LM (1988) Locomotion produced in mesencephalic cats by injections of putative transmitter substances and antagonists into the medial reticular formation and the pontomedullary locomotor strip. J Neurosci 8:2074–2086.

Okura M, Fujiki N, Kita I, Honda K, Yoshida Y, Mignot E, Nishino S (2004) The roles of midbrain and diencephalic dopamine cell groups in the regulation of cataplexy in narcoleptic Dobermans. Neurobiol Dis 16:274–282.

Oleson EB, Gentry RN, Chioma VC, Cheer JF (2012) Subsecond dopamine release in the nucleus accumbens predicts conditioned punishment and its successful avoidance. J Neurosci 32:14804–14808.

Ondo WG, He Y, Rajasekaran S, Le W-D (2000) Clinical correlates of 6-hydroxydopamine injections into A11 dopaminergic neurons in rats: A possible model for restless legs syndrome? Mov Disord 15:154–158.

Orazzo C, Pieribone VA, Ceccatelli S, Terenius L, Hökfelt T (1993) CGRP-like immunoreactivity in A11 dopamine neurons projecting to the spinal cord and a note on CGRP-CCK cross-reactivity. Brain Res 600:39–48.

Pappas SS, Behrouz B, Janis KL, Goudreau JL, Lookingland KJ (2008) Lack of D2 receptor mediated regulation of dopamine synthesis in A11 diencephalospinal neurons in male and female mice. Brain Res 1214:1–10.

Pappas SS, Kennedy T, Goudreau JL, Lookingland KJ (2011) Opioid-mediated regulation of A11 diencephalospinal dopamine neurons: pharmacological evidence of activation by morphine. Neuropharmacology 61:614–621.

Pappas SS, Tiernan CT, Behrouz B, Jordan CL, Breedlove SM, Goudreau JL, Lookingland KJ (2010) Neonatal androgen-dependent sex differences in lumbar spinal cord dopamine concentrations and the number of A11 diencephalospinal dopamine neurons. J Comp Neurol 518:2423–2436.

Paredes RG, Agmo A (2004) Has dopamine a physiological role in the control of sexual behavior? A critical review of the evidence. Prog Neurobiol 73:179–226.

Peyron C, Luppi P-H, Kitahama K, Fort P, Hermann DM, Jouvet M (1995) Origin of the dopaminergic innervation of the rat dorsal raphe nucleus. Neuroreport 6:2527–2531.

Picton LD, Sillar KT (2016) Mechanisms underlying the endogenous dopaminergic inhibition of spinal locomotor circuit function in Xenopus tadpoles. Sci Rep 6:1–15.

Piña-Leyva C, Lara-Lozano M, Rodríguez-Sánchez M, Vidal-Cantú GC, Zavalza-Barrientos E, Jiménez-Estrada I, Delgado-Lezama R, Rodríguez-Sosa L, Granados-Soto V, Florán-Garduño B, González-Barrios JA (2020) Hypothalamic A11 Nuclei Regulate the Circadian Rhythm of the Mechanonociception and the Spinal Clock Gene Transcription through Dopamine Receptor Activation. Preprints Available at: http://dx.doi.org/10.20944/preprints202009.0188.v1.

Pisanello M, Pisano F, Hyun M, Maglie E, Balena A, De Vittorio M, Sabatini BL, Pisanello F (2019) The Three-Dimensional Signal Collection Field for Fiber Photometry in Brain Tissue. Front Neurosci 13:1–16.

Portfors CV (2007) Types and functions of ultrasonic vocalizations in laboratory rats and mice. J Am Assoc Lab Anim Sci 46:28–34.

Premoli M, Memo M, Bonini SA (2021) Ultrasonic vocalizations in mice: relevance for ethologic and neurodevelopmental disorders studies. Neural Regeneration Res 16:1158–1167.

Puglisi-Allegra S, Cabib S (1997) Psychopharmacology of dopamine: the contribution of comparative studies in inbred strains of mice. Prog Neurobiol 51:637–661.

Puhl JG, Mesce KA (2008) Dopamine activates the motor pattern for crawling in the medicinal leech. J Neurosci 28:4192–4200.

Puopolo M (2019) The hypothalamic-spinal dopaminergic system: a target for pain modulation. Neural Regeneration Res 14:925–930.

Qu S, Le W, Zhang X, Xie W, Zhang A, Ondo WG (2007) Locomotion is increased in A11-lesioned mice with iron deprivation: a possible animal model for restless legs syndrome. J Neuropathol Exp Neurol 66:383–388.

Qu S, Ondo WG, Zhang X, Xie WJ, Pan TH, Le WD (2006) Projections of diencephalic dopamine neurons into the spinal cord in mice. Exp Brain Res 168:152–156.

Reinig S, Driever W, Arrenberg AB (2017) The Descending Diencephalic Dopamine System Is Tuned to Sensory Stimuli. Curr Biol 27:318–333.

Robinson DL, Heien MLAV, Wightman RM (2002) Frequency of dopamine concentration transients increases in dorsal and ventral striatum of male rats during introduction of conspecifics. J Neurosci 22:10477–10486.

Rogers JH (1992) Immunohistochemical markers in rat brain: colocalization of calretinin and calbindin-D28k with tyrosine hydroxylase. Brain Res 587:203–210.

Roseberry TK, Lee AM, Lalive AL, Wilbrecht L, Bonci A, Kreitzer AC (2016) Cell-Type-Specific Control of Brainstem Locomotor Circuits by Basal Ganglia. Cell 164:526–537.

Rothwell JC (2011) The motor functions of the basal ganglia. J Integr Neurosci 10:303–315.

Russell FA, King R, Smillie S-J, Kodji X, Brain SD (2014) Calcitonin gene-related peptide: physiology and pathophysiology. Physiol Rev 94:1099–1142.

Schomaker J, Meeter M (2015) Short- and long-lasting consequences of novelty, deviance and surprise on brain and cognition. Neurosci Biobehav Rev 55:268–279.

Schultz W (1997) Dopamine neurons and their role in reward mechanisms. Curr Opin Neurobiol 7:191–197.

Sharma S, Kim LH, Mayr KA, Elliott DA, Whelan PJ (2018) Parallel descending dopaminergic connectivity of A13 cells to the brainstem locomotor centers. Sci Rep 8:1–15.

Sharples SA, Koblinger K, Humphreys JM, Whelan PJ (2014) Dopamine: a parallel pathway for the modulation of spinal locomotor networks. Front Neural Circuits 8:1–16.

Skagerberg G, Björklund A, Lindvall O, Schmidt RH (1982) Origin and termination of the diencephalo-spinal dopamine system in the rat. Brain Res Bull 9:237–244.

Skagerberg G, Lindvall O (1985) Organization of diencephalic dopamine neurones projecting to the spinal cord in the rat. Brain Res 342:340–351.

Smith KS, Bucci DJ, Luikart BW, Mahler SV (2016) DREADDS: Use and application in behavioral neuroscience. Behav Neurosci 130:137–155.

Takada M (1990) The A11 catecholamine cell group: another origin of the dopaminergic innervation of the amygdala. Neurosci Lett 118:132–135.

Takada M (1993) Widespread dopaminergic projections of the subparafascicular thalamic nucleus in the rat. Brain Res Bull 32:301–309.

Takada M, Li ZK, Hattori T (1988) Single thalamic dopaminergic neurons project to both the neocortex and spinal cord. Brain Res 455:346–352.

Tapper AR, Molas S (2020) Midbrain circuits of novelty processing. Neurobiol Learn Mem 176:1–10.

Thirumalai V, Cline HT (2008) Endogenous dopamine suppresses initiation of swimming in prefeeding zebrafish larvae. J Neurophysiol 100:1635–1648.

Thurston EMS, Molina LA, Le VA, Cheng N, Murari K, Whelan PJ (2021) Population-level fiber photometry recording of A11 activity in different behavioral contexts [abstract]. In: Neuroscience 2022 , November 8-11 2022, Chicago, IL.

Tian L, Hires SA, Mao T, Huber D, Chiappe ME, Chalasani SH, Petreanu L, Akerboom J, McKinney SA, Schreiter ER, Bargmann CI, Jayaraman V, Svoboda K, Looger LL (2009) Imaging neural activity in worms, flies and mice with improved GCaMP calcium indicators. Nat Methods 6:875–881.

Tillet Y (1994) Catecholaminergic neuronal systems in the diencephalon of mammals. In: Phylogeny and development of catecholamine systems in the CNS of vertebrates (Reiner A, ed), pp 207–246. University of Cambridge Press.

van den Pol AN (1986) Tyrosine Hydroxylase lmmunoreactive Neurons Throughout the Hypothalamus Receive Glutamate Decarboxylase lmmunoreactive Synapses: A Double Pre-embedding lmmunocytochemical Study with Particulate Silver and HRP. J Neurosci:877–891.

Walf AA, Frye CA (2007) The use of the elevated plus maze as an assay of anxiety-related behavior in rodents. Nat Protoc 2:322–328.

Wang D, Sutherland D, McErlane S, Soja P (2005) Long-lasting reduction in rat sensory thresholds following ablation of diencephalic A11 dopamine (DA) nuclei [abstract]. In: Neuroscience 2005 , November 12-16 2005, Washington, DC.e

Wang H, Liang S, Burgdorf J, Wess J, Yeomans J (2008) Ultrasonic vocalizations induced by sex and amphetamine in M2, M4, M5 muscarinic and D2 dopamine receptor knockout mice. PLoS One 3:e1893.

Weiner B, Hertz S, Perets N, London M (2016) Social Ultrasonic Vocalization in Awake Head-Restrained Mouse. Front Behav Neurosci 10:236.

Whelan P, Bonnot A, O'Donovan MJ (2000) Properties of rhythmic activity generated by the isolated spinal cord of the neonatal mouse. J Neurophysiol 84:2821–2833.

Whelan PJ (1996) Control of locomotion in the decerebrate cat. Prog Neurobiol 49:481–515.

Whitney G, Coble JR, Stockton MD, Tilson EF (1973) Ultrasonic emissions: Do they facilitate courtship of mice? J Comp Physiol Psychol 84:445–452.

Wirtshafter D, Sheppard AC (2001) Localization of GABAB receptors in midbrain monoamine containing neurons in the rat. Brain Res Bull 56:1–5.

Yamaguchi T, Ozawa H, Yamaguchi S, Hamaguchi S, Ueda S (2021) Calbindin-Positive Neurons Co-express Functional Markers in a Location-Dependent Manner Within the A11 Region of the Rat Brain. Neurochem Res 46:853–865.

Yamamoto K, Vernier P (2011) The evolution of dopamine systems in chordates. Front Neuroanat 5:1–21.

Yasui Y, Nakano K, Mizuno N (1992) Descending projections from the subparafascicular thalamic nucleus to the lower brain stem in the rat. Exp Brain Res 90:508–518.

Zhao H, Zhu W, Pan T, Xie W, Zhang A, Ondo WG, Le W (2007) Spinal cord dopamine receptor expression and function in mice with 6-OHDA lesion of the A11 nucleus and dietary iron deprivation. J Neurosci Res 85:1065–1076.

Zingg B, Chou X-L, Zhang Z-G, Mesik L, Liang F, Tao HW, Zhang LI (2017) AAV-Mediated Anterograde Transsynaptic Tagging: Mapping Corticocollicular Input-Defined Neural Pathways for Defense Behaviors. Neuron 93:33–47.

APPENDICES

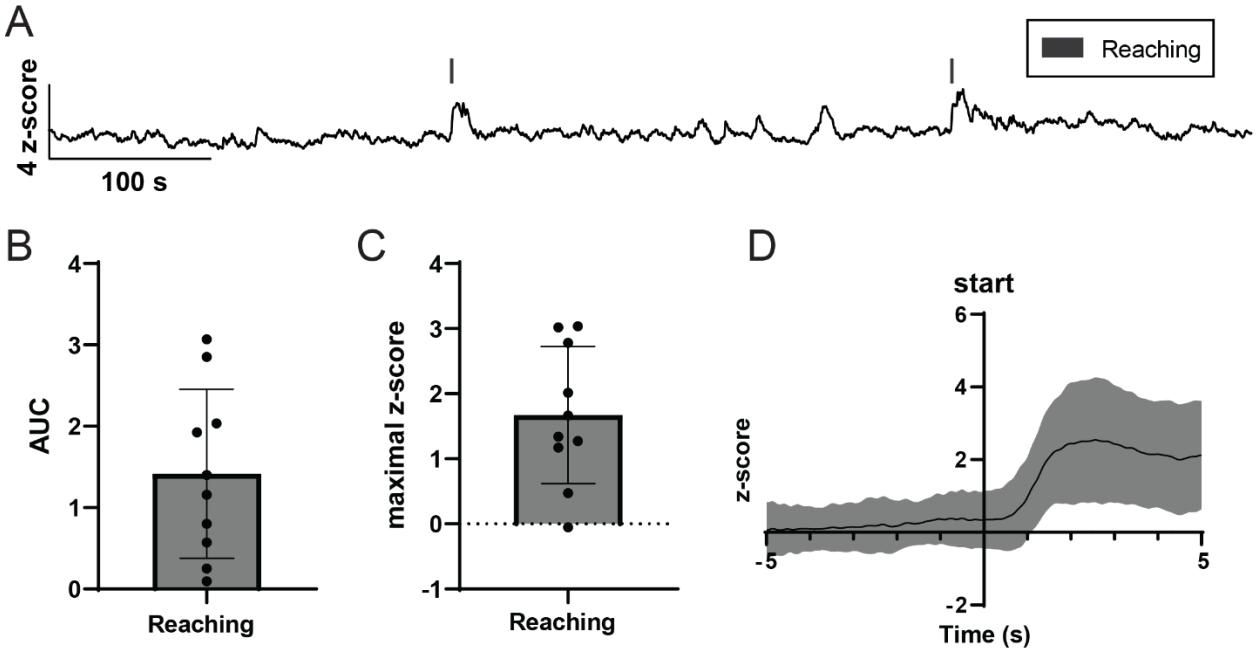

Appendix A. A) Sample trace showing the A11's activity during the periods of reaching. **B)** Area under the curve for the reaching behaviour. The fluorescence returns to baseline within 10 - 15 s. **C)** Average maximal fluorescence achieved during the reaching behaviour. **D)** Onset of reaching behaviour at time = 0 demonstrating an increase in A11 fluorescence when reaching occurs.

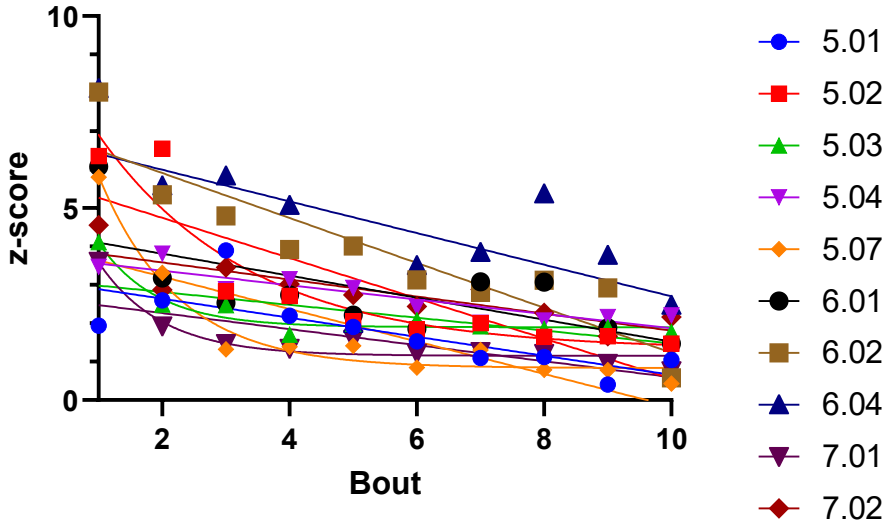

Appendix B. Individual-level data for the novel female maximal fluorescence decay. Four of ten mice fit with an exponential decay (mouse identifiers 5.02, 5.03, 5.07, 7.01), while the remaining six were fit with a linear regression.

Appendix C: The Spinally-Projecting Population of Cells Within the A11 Region and their Contribution to the Production of Locomotor Behaviours

Elizabeth M.S. Thurston, Sandeep Sharma, Patrick J. Whelan

INTRODUCTION

The A11 nucleus, found within the posterior hypothalamus, has recently been postulated to be involved in locomotor behaviours (Dahlström and Fuxe, 1964; Koblinger et al., 2018). This region, which is both glutamatergic and dopaminergic, is defined by a distinct population of dopaminergic cells (approximately 130 cells in the mouse) of which a subset project to all levels of the spinal cord (Dahlström and Fuxe, 1964; Hökfelt et al., 1976; Qu et al., 2006; Pappas et al., 2010; Koblinger et al., 2014; Fougère et al., 2021).

A facet of A11 research has implicated this region in nociception; the electrical stimulation of the A11 decreases nociceptive responses, while the lesioning of this region increases sensitivity to stimuli (both noxious and innocuous) (Fleetwood-Walker et al., 1988; Charbit et al., 2011). Additional research has suggested that the A11 plays a role in cataplexy, migraine, defecation, and sociosexual behaviours (Okura et al., 2004; Bharati and Goodson, 2006; Charbit et al., 2009; Nakamori et al., 2019). More recently, work by Koblinger et al. (2018) has demonstrated that the photostimulation of the dopaminergic cell population of the A11 results in increased locomotor activity. Despite the well-characterized spinally-projecting A11 cells, there has not been any work to specifically elucidate the role of these descending fibres, in nociception or otherwise, as work has focused on general stimulation or inhibition of the A11 as a whole or exclusively the dopaminergic populations.

Given that dopamine and DAergic receptors modulate spinal motor circuits, promote ongoing locomotor activity, and that the A11 is the primary direct source of spinal dopamine in rodents, it is possible that this A11-spinal cord circuit could be responsible for eliciting these locomotor behaviours (Madriaga et al., 2004; Qu et al., 2006; Han et al., 2007; Sharples et al., 2014). These spinal projections reach all levels of the spinal cord; they are localized in the superficial layers of the dorsal horn, intermediolateral cell column, and central gray (Cechetto

and Saper, 1988; Takada, 1990). These long projections collateralize at all levels of the spinal cord (Skagerberg and Lindvall, 1985).

Previous work by Koblinger et al. (2018) targeted the entire bilateral dopaminergic A11 nucleus using a viral approach and bilateral optogenetic stimulation. My work was built on the concept that the stimulation of the A11 region can produce locomotor behaviour, by specifically activating the descending A11 cells (Koblinger et al., 2018). An intersectional viral approach allowed me to introduce channelrhodopsin-2 (ChR2) into the A11 cells that project directly to the thoracolumbar spinal cord, and exclusively photostimulate these connections after implantation of an optic fibre. This was accomplished by a Cre-driver system (Gore et al., 2013). The use of an intersectional viral approach is dependent on the Cre-lox system. Cre recombinase is an enzyme derived from P1 bacteriophage-derived recombinase, which allows it to perform DNA recombination (McLellan et al., 2017). The specificity of Cre is dictated by the promoter or enhancer sequences that are included, which allows for targeting specific cell types or regions (McLellan et al., 2017). Cre targets loxP sites, which bind Cre and allow the crossing over of genetic material (McLellan et al., 2017). Another term to indicate Cre-inducible elements in a viral construct is DIO, a double-floxed inverse orientation element (Haggerty et al., 2020).

I chose to target the spinally-projecting A11 cell population for optogenetic stimulation to determine if this pathway was capable of eliciting locomotor behaviours. This experiment used an intersectional viral approach that consisted of an injection of a retrograde Cre-containing virus into the spinal cord and a Cre-inducible channelrhodopsin virus into the A11 region. This approach allows the specific optogenetic stimulation of A11 cells that project to the thoracolumbar spinal cord regardless of cell identity, rather than using a TH-Cre mouse line that would target dopaminergic neurons.

METHODS

Animals

Male C57BL/6 mice eight to ten weeks of age at the date of surgery (Charles River Laboratories, Senneville, QC) were used in this experiment, apart from Rosa-GFP mice being used for the early viral validations. Animal use and surgery were performed in accordance with animal use guidelines set by the University of Calgary Health Science Animal Care Committee

(Protocol number AC0019-0035). Animals were single-housed following surgery in a 12:12 light:dark cycle (lights on and off at 7 a.m. - 7 p.m.) with ad libitum access to water and mouse chow. 11 C57/BL6 male mice were used for the experiment and seven male Rosa-GFP reporter mice were used for the viral validation. Of the former group, eight mice were excluded due to inaccurate targeting of the fibre-optic cannula implantation.

Experimental Methods

Confirmation of Virus

Two different retrograde Cre-carrying viruses were compared for use in the intersectional viral approach. A CAV2-Cre virus (Montpellier, 13.0e+12 virus molecules/mL) or a retrograde Cre-carrying AAV virus (pAAVrg-EF1a-mCherry-IRES-Cre, Addgene #55632-AAVrg, lot #v15410,1.30e+13 virus molecules/mL) were injected (27.6 nL per injection site, 441.6 nL total) into the thoracolumbar region of male Cre-inducible Rosa-GFP mice (Fig. 3.1A). Following transfection for 3 - 4 weeks, the mice were perfused, and tissue was processed and imaged as described below. GFP-positive cells were manually counted. There were comparable numbers of GFP-positive cells within the A11 region when comparing the two viral constructs (Fig. 3.1B-D), suggesting that the spinally-projecting A11 cells were transfected at comparable rates. As a result, the retrograde AAV was chosen for the intersectional approach because of its mCherry tag.

Surgical Methods

Mice underwent two surgeries, one in the spinal cord and one in the brain, specifically targeting the spinally-projecting A11 cells using an intersectional viral approach (Fig. 3.2A-B). For the spinal cord injection, mice were anaesthetised under isoflurane (4-5% induction, 1% maintenance) via medical-grade oxygen flowing at 0.5 L/min and administered subcutaneous lidocaine (dose: 6 mg/kg, concentration: 20 mg/mL) and buprenorphine (dose: 0.05 mg/kg, concentration: 0.03 mg/mL) for analgesia. Mice were confirmed to be in a surgical plane of anaesthesia via foot or tail pinch. The surgical site was shaved and disinfected with betadine and 70% ethanol. A partial laminectomy exposed the thoracolumbar spinal cord (between spinal cord segments T13 and L2 due to increased DA responsiveness), where the cord was injected with a retrograde Cre-carrying AAV virus bilaterally (pAAVrg-EF1a-mCherry-IRES-Cre, Addgene

#55632-AAVrg, lot #v15410,1.30e+13 virus molecules/mL, eight injection sites, 16 injections total, see Figure 13B) bilaterally (Christie and Whelan, 2005). Following each injection, there was a one-minute wait to allow diffusion of the virus. After the spinal injections were performed, Surgicell (Ethicon Inc., Somerville, NJ, USA) was placed above the cord, and the overlying muscles and skin were sutured. Animals were monitored for 48 hours following this procedure.

Seven days following this surgery, mice underwent a viral brain injection. Mice were induced and administered medication as stated previously and were confirmed to be in a surgical plane of anaesthesia. Mice were then placed in a stereotaxic rig (Stoelting Co., Wood Dale, IL) to secure the head. The scalp was disinfected with betadine and 70% ethanol, and the skull was exposed. A small hole was drilled at the injection coordinates, and using a pulled glass pipette, mice were injected with a virus containing a Cre-inducible channelrhodopsin protein (AAV9/pAAV-Ef1a-DIO-ChR2-eYFP, Addgene #20298-AAV9, lot # v45835, titer: 1.8e+13 virus molecules per mL) or a control virus without ChR2 (AAV9/pAAV-Ef1a-DIO-eYFP, Addgene # 27056-AAV9, lot # V44841, 2.20e+13 virus molecules/mL) unilaterally into the A11 nucleus [stereotaxic coordinates: AP 2.2 mm, ML ± 0.11 mm, DV -2.7 mm from dura; coordinates adapted from Koblinger et al. (2018)]. Then, a mono fibre-optic cannula (Doric Lenses, Quebec, QC, MFC_200/240-0.22_4mm_MF2.5_FLT) was implanted just above the right A11 (stereotaxic coordinates: AP 2.30mm, ML - 0.10mm, DV -3.5mm from dura) and affixed to the skull using a two-step dental cement process [Metabond (K Dental Inc., Markham, ON) and Dentsply (Zahn Canada, Niagara-on-the-Lake, ON)]. Animals were monitored for 48 hours following the surgery. Experiments did not begin until four weeks after the first surgery, to allow for effective viral transfection and expression.

Behavioural Experiments

Laser Information

The laser (473 nm, LRS-0473-GFM, Laserglow Technologies) was controlled by a Master 8 pulse stimulator (A.M.P.I., Jerusalem, Israel) outputting TTL pulses (20 Hz, 10 ms pulse width, 10 mW) (Koblinger et al., 2018). The laser strength was measured using a Digital Optical Power and Energy Meter (PM100D, Thorlabs, Newton, NJ) paired with the S132C Photodiode Power Sensor (Thorlabs, Newton, NJ) and laser output was adjusted to measure 10 mW at the patch cord tip.

Collection of Behavioural Data

All the behavioural data were collected from a top-down view (SuperCircuits, PC165DNR camera, Austin, TX, 30fps) using TopScan software (CleverSys, Reston, VA).

Open Field Experiment

The open field allows for the measurement of locomotor behaviours (Gould et al., 2009). Following the three-week incubation period, mice were habituated to handling for a minimum of five days and to the optogenetic fibre patch cord and the open field (OF; see figure 3.2D for diagram) for a minimum of three days. On the experimental day, the mouse was placed in the OF (50 x 50 x 50 cm) with a fibre attached and was left for 10 minutes. Then optogenetic stimulation occurred at a frequency of 20 Hz (10 ms pulse width, 10 mW) ON/OFF for 180 s each for 20 mins. The mouse was then disconnected from the fibre and returned to its home cage.

Elevated Plus Maze

Mice were placed in an unhabituated elevated plus maze (EPM; open arms: 8.5 x 21.5 cm, closed arms: 8.5 x 21.5 x 22 cm; see figure 3.2G for diagram) adapted for use with a patch cord. This test was based on previous reports (Walf and Frye, 2007). The mouse was introduced to the maze facing toward a closed arm and was allowed to freely wander for nine minutes. The first and last three minutes constituted a laser OFF period, with the middle three minutes comprising a laser ON period (20 Hz, 10 ms pulse width, 10 mW). The time spent in the open and closed arms was compared between the laser ON and OFF periods.

Light/Dark Test

Mice were placed in an unhabituated light/dark box optimized for use with a patch cord (dimensions: 42.5 cm x 42.5 cm x 30.9 cm). Mice were introduced to the dark side of the arena and left to wander freely for nine minutes. The first and last three minutes constituted a laser OFF period, with the middle three minutes constituting a laser ON period (20 Hz, 10 ms pulse width, 10 mW). The time spent in the bright and dark halves of the arena was compared between the laser ON and OFF periods. This test served as a measure of unconditioned anxiety given the trade-off between wanting to remain in a safe, dimly-lit space and the drive to explore a new environment despite an aversion to bright light (Arrant et al., 2013).

Real-Time Place Preference/Aversion

Open Field

Based on the work by Cassidy et al. (2019), the mice were placed in the open field and left to explore for 10 minutes (Fig. 3.2J). Using the TopScan system, one half of the arena was designated as the laser ON region and the other half as the laser OFF region. The tracking software then tracked the mouse during the 10-minute test, and when the mouse was on either side of the arena, the laser was either set to be ON or OFF. This test allowed us to assign a positive or negative valence to the photostimulation, depending on the time spent on either side of the open field arena. The arena was uncued, and as such, the test was also run in a cued environment.

Cued Two-Chamber Arena

The cued two-chamber arena consisted of two chambers with a corridor connecting them (total dimensions: 25.5 cm x 45 cm x 26 cm, chamber dimensions: 20.3 cm x 17.9 cm x 26 cm, see figure 3.2M for diagram). Each chamber had a different pattern on the wall. One chamber was randomly designated as laser ON and the other as laser OFF. The mouse was placed in this arena and allowed to freely roam for 10 minutes (Bimpisidis et al., 2020). The laser was ON when the mouse was tracked in the chamber designated as the laser ON (20 Hz, 10 ms pulse width, 10 mW). This test allowed us to determine if the laser stimulation was a positive or negative stimulus or if the mouse was indifferent to the stimulation, depending on the time spent in either chamber.

Post-hoc Processing

Exclusion Criteria

Post-hoc analyses were performed to exclude mice that had off-target injections from subsequent data analysis. Mice with fibre-optic cannulas further than 1 mm away from the A11 region were excluded. In addition, mice with fibre-optic cannulas too rostral or caudal (targeting the A13 or rostral periaqueductal gray) were also excluded, leaving an n = 3 remaining mice (2 ChR2 mice, one control eYFP mouse, representative image in figure 3.2C). There were no apparent effects on behaviour during photostimulation of the mice that were later excluded.

Immunohistochemical Protocols

To determine what proportion of targeted spinally projecting A11 cells were DAergic, immunohistochemical methods were used to stain for TH. The brains were sliced coronally using a cryostat (Leica CM1850 UV, Leica Biosystems, Wetzlar, Germany) at 40 μm thickness, and slices were collected in a three-series in a well plate to free-float in 1x phosphate-buffered saline (PBS). For the immunohistochemical staining, slices were washed in 1x PBS at room temperature (RT), then washed in 0.5% triton in PBS (PBST) at RT. Then slices were placed in block (0.3% PBST and 5% donkey serum) at RT and subsequently placed in a primary solution (1:500 Ch-anti-GFP, 1:1000 Sh-anti-TH or 1:1000 Rb-anti-TH diluted in block, see table 3.1) overnight at RT. The next day, slices were again washed in 1x PBS then placed in secondary (1:1000 Dk-anti-Ch-488, 1:1000 Dk-anti-Sh-647 or 1:1000 Dk-anti-Rb-647, see table 3.2) diluted in block (0.3% PBST and 5% donkey serum), and finally washed in 1x PBS at RT. Slices were mounted on slides and coverslipped with VectaShield (Vector Labs, Burlingame, CA).

Table C3.1. Primary antibodies.

Antigen	**Lab Code**	**Commercial Source**	**Dilution and Incubation time**	**Donor Species**
TH	ab112	Abcam	1:1000, overnight	rabbit
TH	AB1542	Millipore	1:500, overnight	sheep
GFP	GFP-1020	Aves Labs	1:500, overnight	chicken

Table C3.2. Secondary antibodies.

Secondary Antibody	**Lab Code**	**Commercial Source**	**Dilution**
Alexa-488-conjugated donkey anti-chicken	703-545-155	Jackson ImmunoResearch	1:1000
Alexa-647-conjugated donkey-anti-sheep	A21448	Life Technologies	1:1000
Alexa-647-conjugated donkey-anti-rabbit	A31573	Life Technologies	1:1000

Images were taken on an epifluorescent microscope (5x to 20x magnification, Olympus BX51, Tokyo, Japan; TXRED 4040B - OMF excitation (ex) 562 nm - emission (em) 624 nm, FITC 3540B - OMF excitation 482 nm - emission 536 nm) with a camera (MicroPublisher 3.3 RTV, Teledyne Q Imaging, Surrey, BC), or the Slide Scanner (2x and 10x magnification, Olympus VS110-S5, Tokyo, Japan; DAPI ex 387/11 nm – em 440/40 nm; FITC ex 485/20 nm – em 525/30 nm; TRITC ex 560/25 nm – em 607/36 nm; Cy5 ex 650/13 nm – em 684/24 nm) with a camera (Olympus XC10 and XM10).

Behavioural Analysis

Behaviour was analyzed and categorized using TopScan and graphing was performed using GraphPad Prism 9.

Statistical Analysis

For the viral validation, D'Agostino-Pearson normality test was used, followed by an unpaired two-tailed t-test. For behavioural data, no statistical analysis beyond descriptive statistics was undertaken due to the small sample size following the exclusion process.

RESULTS

Viral Validation

I validated two retrograde viruses (CAV-2 Cre and a retrograde AAV) to determine their efficiency in targeting spinally-projecting A11 cells. Cell counts were performed, and an unpaired t-test was run. GFP-positive cells counted within the A11 represented the cell population that had successfully been targeted with Cre via either of the viruses and was expressing the Cre-inducible GFP (Fig. 3.1C-D). There was no significant difference in GFP-positive cells between the retrograde AAV and the CAV2-Cre virus [unpaired t-test, $p = 0.4470$, $t = 0.7774$, $df = 18$, $n = 12$ (AAV), $n = 8$ (CAV-2 Cre)]. The retrograde AAV was chosen for further work because the mCherry reporter served as a secondary confirmation that the retrograde virus had reached the region of interest.

Targeting Efficiency

Given there were few mice with on-target injections or implantations (n = 2 for the experimental group, n = 1 for the control group), no statistical tests were run on the data. As a result, only descriptive statistics are presented. Values are mean ± standard deviation.

Open Field

In the open field test (fig. 3.2D), two parameters were investigated and compared between groups: duration of locomotor behaviours (fig. 3.2E) and in-place activity (Fig. 3.2F; Table 3.3).

Table 3.3. The average duration of behaviours (seconds) during optogenetic stimulation parameters.

	Laser	**ChR2 (n = 2)**	**eYFP (n = 1)**
Locomotion	Baseline	19.68 ± 0.52	54.02
	ON	23.65 ± 3.06	37.66
	OFF	24.76 ± 1.35	28.51
In-Place Activity	Baseline	32.67 ± 0.84	105.38
	ON	28.31 ± 1.93	127.09
	OFF	26.83 ± 2.19	130.06

Elevated Plus Maze

In the EPM, time in open arm was investigated between the two groups [ChR2 (n = 2): OFF = 13.68 ± 3.92 s, ON = 15.48 ± 6.85 s, OFF = 24.46 ± 19.11 s, eYFP (n = 1): OFF = 15.88 s, ON = 15.78 s, OFF = 0.00 s] as a measure of exploratory behaviours in which the mice were engaging (Fig. 3.2H).

Dark/Light Test

In the dark/light test, time in the light side of the arena was compared between the two groups [ChR2 (n = 2): OFF = 61.25 ± 15.37 s, ON = 71.27 ± 30.91 s, OFF = 55.31 ± 11.45 s, eYFP (n = 1): OFF = 40.14 s, ON = 0.40 s, OFF = 69.77 s] to determine changes in anxiety-like behaviours with photostimulation (Fig. 3.2I).

Real-Time Place Preference/Aversion in the OF

In the open field arena-based real-time place preference/aversion test (fig. 3.2J), time spent in each chamber [ChR2 (n = 2): ON = 335.59 ± 3.19 s, OFF = 264.38 ± 3.18 s, eYFP (n = 1): ON = 487.15 s, OFF = 112.91 s; fig. 3.2K] and time spent locomoting in each side of the arena [ChR2 (n = 2): ON = 87.69 ± 38.65 s, OFF = 78.60 ± 18.52 s, eYFP (n = 1): ON = 22.59 s, OFF = 33.80 s, fig. 3.2L] were investigated.

Real-Time Place Preference/Aversion in Two-Chambered Arena

In the two-chambered arena real-time place preference/aversion test, time in each of the chambers [ChR2 (n = 2), ON = 232.61 ± 44.17 s, OFF = 232.94 ± 18.31 s, eYFP (n = 1), ON = 165.27 s, OFF = 144.88 s; fig. 3.2N] and time spent locomoting in each chamber [ChR2 (n = 2), ON = 68.62 ± 4.79 s, OFF = 54.42 ± 9.82 s, eYFP (n = 1), ON = 38.14 s, OFF = 38.74 s; fig. 3.2O] were investigated.

DISCUSSION

The present work builds on work by Koblinger et al. (2018), where it was determined that the optogenetic stimulation of the dopaminergic cells of the A11 produces an increase in locomotor and in-place activities. While this suggests that the A11 is sufficient to produce locomotor behavior, the A11 circuits critical for this behavior remain to be elucidated. The A11-spinal cord is a likely target since locomotor centres are present, dopamine receptors are found, and the A11 projects to all spinal cord segments. I therefore targeted the spinally-projecting cell population of this region, focusing on the A11-spinal cord circuit. I used an intersectional viral approach to target the spinally projecting (or descending) A11 cells for photostimulation. I used the same stimulation parameters as Koblinger et al. (2018), because the parameters were tested on brain slices, and Na+ spikes were recorded at frequencies up to 20 Hz during whole cell patching. While Koblinger et al. (2018) targeted the dopaminergic cell population using a TH-Cre mouse line, my work instead focused simply on the projection-identity of the cells rather than cell-type identity by forgoing the use of a Cre mouse line. Though the large descending A11 neurons are dopaminergic, a known subset of TH-positive cells project to the spinal cord but the current work does not suggest any cell type-specific results, only pathway-specific (Qu et al., 2006; Koblinger et al., 2014).

The retrograde viral validation work provides further support that only a subset of A11 TH-positive cells projects to the thoracolumbar spinal cord, in line with previous work showing that between 40 - 60 % of the large multipolar TH-positive cells in a single slice are labelled by a spinally-injected retrograde tracer (Qu et al., 2006; Pappas et al., 2010; Koblinger et al., 2014).

Based on previous work by Koblinger et al. (2018), I expected that within the open field test, there would be an increase in locomotor behaviours during periods of photostimulation in the ChR2 group. As a result of our small sample sizes, there can only be general conclusions drawn, and further investigation is required. There was no obvious increase in the time spent locomoting, and similarly no change in time spent engaging in in-place activity, which does not currently support the hypothesis that the descending projections of the A11 contribute to increased locomotor or in-place activity behaviours. I chose to explore the effects on locomotor and non-locomotor behaviours within the context of an elevated plus maze with concurrent stimulation of the descending A11 cells. I expected that, if the stimulation of the A11 induced exploratory locomotor behaviours, we would see an increase in time spent in the open arms and/or locomotor behaviours during the laser ON period. I did not see any obvious trends. In addition, the stimulation of the A11 did not seem to influence the time spent exploring the light side in the light/dark test, suggesting no changes in anxiety between laser ON/OFF periods.

Given that the A11 is also involved in pain processing (Puopolo, 2019), I felt it important to determine if the optogenetic stimulation of the A11 induced feelings of discomfort or unpleasantness. More specifically, the A11 could be a therapeutic target for migraine or restless leg syndrome (Charbit et al., 2011; Kagan et al., 2013; Abdallah et al., 2015; Liu et al., 2019; Puopolo, 2019). Therefore, as a potential target for therapy, it is important that the manipulation of this region does not induce painful or unpleasant sensations to explore future roles in therapies or medications. The two tests I chose to test the valence of stimulation of the pathway were: examining real-time place preference or aversion in a cued two-chamber arena, as well as in an uncued open field arena. In both setups, the mouse would avoid the side paired with optogenetic stimulation if the manipulation was unpleasant or would increase its time spent on the paired side if the stimulation was enjoyable. I did not observe any clear preference or avoidance of the paired side of either arena, which could suggest that I require a larger number of subjects to tease apart any preferences and/or the mice were indifferent to the stimulation of the descending A11

neurons. In addition, it is possible that the cells were not sufficiently illuminated to induce activation of the A11-spinal cord cells; however, the manual confirmation of fibre-optic cannula depth and subsequent exclusion of mice with fibre-optic cannulas > 1 mm from the A11 region suggests that this was not the reason of lack of behavioural responses.

Though the results discussed in this paper do not suggest that the descending A11 cells produce locomotor behaviours when optogenetically stimulated, it is important to note that there are finer, more dextrous skilled movements that were not evaluated such as grasping or stepping patterns that could be affected by optogenetic stimulation.

In addition, the work presented here makes use of optogenetic stimulation of a small subset of the A11 descending cells; within a mouse, it is unlikely that the entire extent of the A11 descending cells were photostimulated within the range of the implanted fibre-optic cannula. As such, it is possible that a sufficient proportion of descending cells to produce locomotor behaviours was not stimulated. Therefore, further work may want to make use of a DREADD approach to ensure the stimulation of the entirety of the descending cell population of this region. Not only is the process less invasive, but there would be the ability to target the entire rostrocaudal extent of the A11, the chemogenetic stimulation would allow for a more naturalistic firing rate, and fewer mice would be excluded due to inaccurate targeting (Smith et al., 2016). The only caveats to using DREADDs would be the loss of temporal control offered by optogenetics because intraperitoneal injection of the clozapine-N-oxide ligand takes approximately 10 minutes to produce its effects and can last 40 - 70 minutes (Smith et al., 2016).

In the future, it is worthwhile to add to the current data set to reach a more fulsome conclusion as to whether the descending A11 cells are responsible for locomotor behaviours. However, recent work in our lab has identified a non-direct locomotor pathway which could be the alternative route through which A11 exerts its effects on locomotor behaviour (Grams et al., 2021). This is in line with the work presented in Chapter 2, suggesting that the A11's activity correlates with novelty and investigation more than locomotor behaviours. The addition of female mice will also help to consider whether the stimulation of this region elicits different behaviours between the two sexes.

CONCLUSION

Future work is needed to bolster the sample size of this work to conclusively determine whether the descending population of the A11 nucleus can elicit locomotor behaviours during optogenetic stimulation.

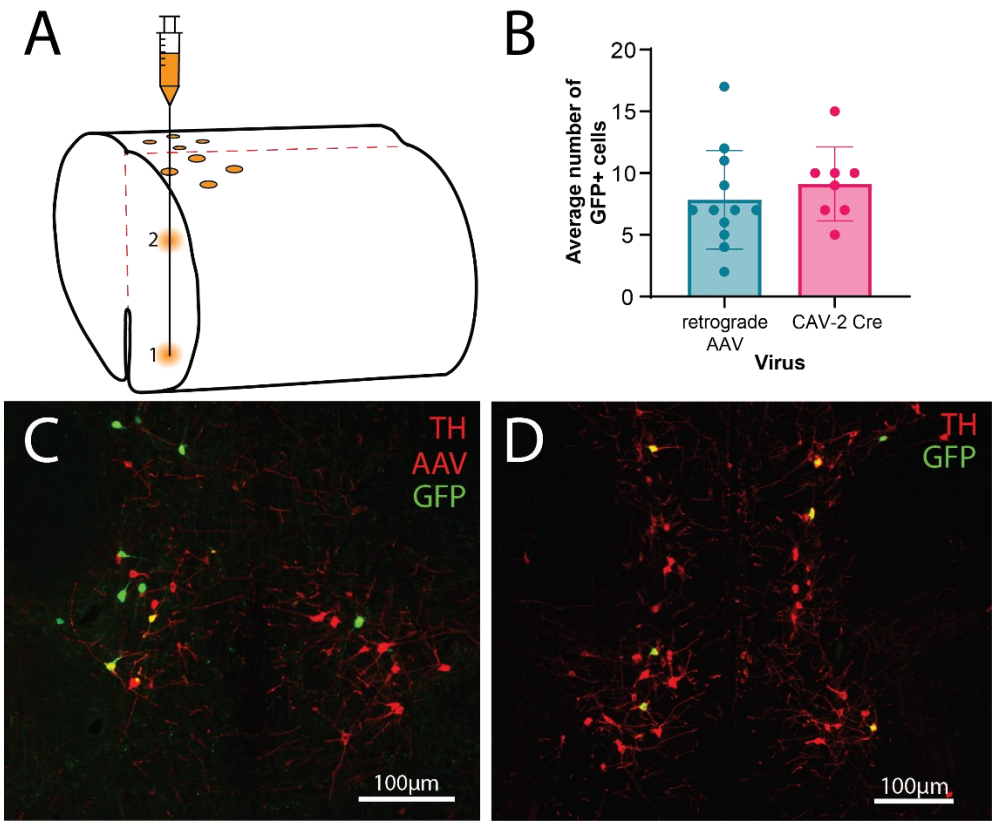

Figure C3.1. Validation of retrograde viruses. **A)** Diagram demonstrating viral spinal cord injections in Rosa-GFP mice at the level of the thoracolumbar spinal cord. **B)** Comparison of the average number of GFP-positive cells at the level of the A11 region between the two viruses used. No significant difference was found (unpaired two-tailed t-test, $p = 0.4470$, $t = 0.7774$, $df = 18$). GFP+ cells indicate spinally-projecting A11 cells that have successfully incorporated the viruses. **C)** Representative image of the A11 region showing a brain injected with a retrograde AAV. TH in red labels dopaminergic cells of the A11, while GFP in green shows cells expressing the retrograde virus. **D)** Representative image of the A11 region showing a brain injected with a retrograde CAV-2 Cre virus. TH in red labels dopaminergic cells of the A11, while GFP in green shows cells expressing the retrograde virus. In D, the AAV used also contained an mCherry reporter.

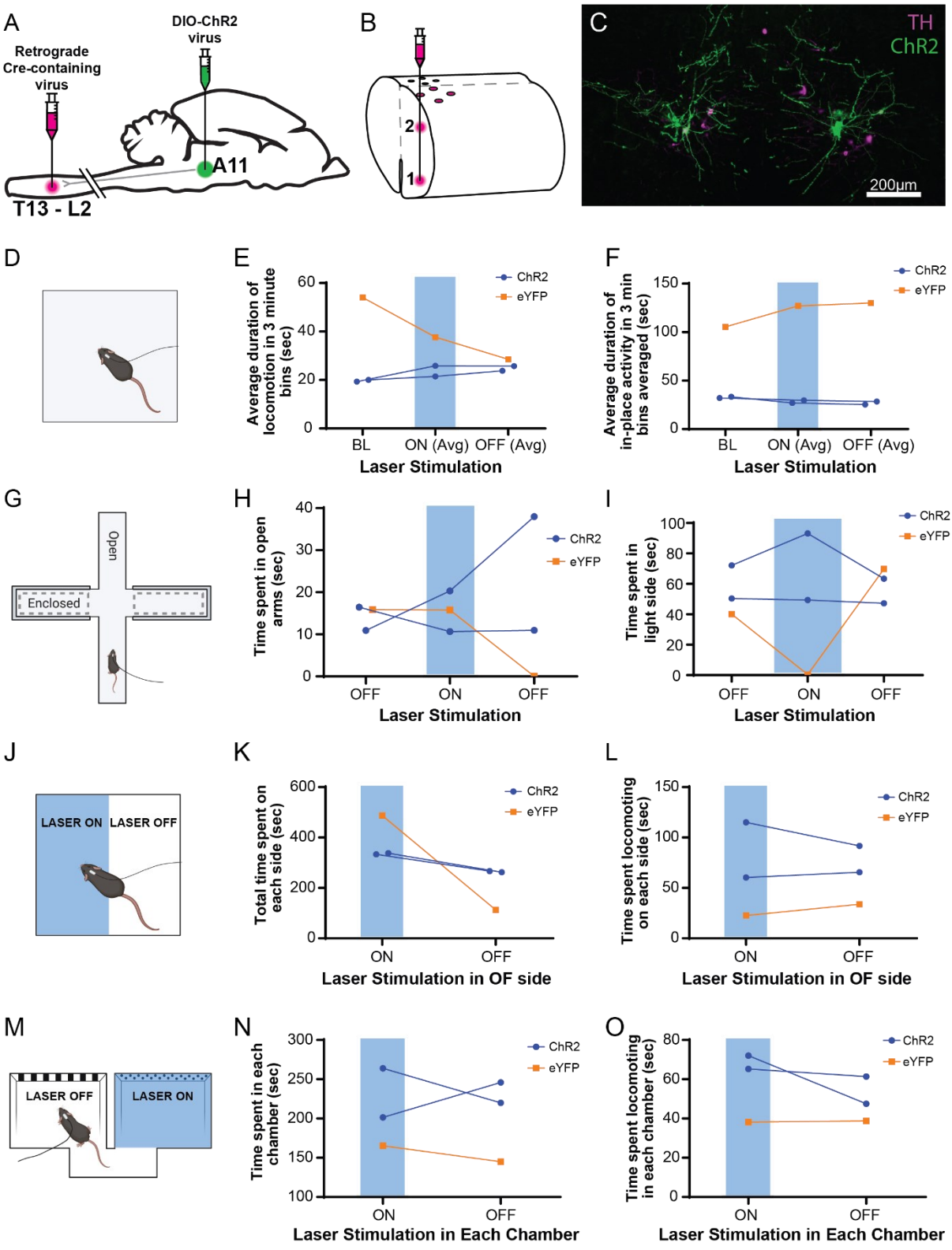

Figure C3.2. The behavioural responses in a variety of contexts during A11 descending fibre photostimulation. **A)** Diagram showing the intersectional viral approach employed. First, a retrograde Cre-containing AAV is injected into the thoracolumbar spinal segments (between T13

and L2). A week later, a Cre-inducible (DOI) channelrhodopsin-2 (ChR2) AAV is injected into the A11 region. **B)** Diagram showing the injection locations for the retrograde AAV into the spinal cord. Each location (orange circle) is injected at two depths. **C)** Representative immunohistochemical staining of the A11 region (indicated by tyrosine hydroxylase staining in magenta) showing successful expression of the Cre-inducible ChR2 virus (in green). **D)** Diagram of the open field (OF) test. **E)** Graph of the OF comparing the duration of locomotion during a 3-minute baseline (BL) compared to the average duration of locomotor behaviour during 3-min periods of laser ON/OFF. The experimental group is in blue, while the control group is in orange. The blue segment indicates the period of laser ON. **F)** Graph of the OF comparing the duration of in-place activity during a 3-minute baseline (BL) compared to the average duration of in-place activity during 3-min periods of laser ON/OFF. **G)** Diagram of the elevated plus maze (EPM). **H)** Graph of the EPM demonstrating the difference in time spent exploring the open arms during the 9-minute test (3 minutes laser OFF, ON, OFF). **I)** Time spent in the illuminated side of the dark/light chamber during the 9-minute test according to laser ON/OFF. **J)** Diagram of the real-time place preference/aversion test in the open field arena (RTPPA-OF). **K)** Total time spent in the RTPPA-OF test on either side of the testing arena, associated with a laser ON or OFF condition. **L)** Total time spent locomoting on either side of the RTPPA-OF arena, associated with a laser ON or OFF condition. **M)** Diagram of the two-chambered real-time place preference/aversion test (2CH-RTPPA). **N)** Total time spent in the 2CH-RTPPA test on either side of the testing arena, associated with a laser ON or OFF condition. **O)** Total time spent locomoting on either side of the 2CH-RTPPA arena, associated with a laser ON or OFF condition.